Atmos. Chem. Phys., 12, 5077–5098, 2012
www.atmos-chem-phys.net/12/5077/2012/
doi:10.5194/acp-12-5077-2012

Atmospheric Chemistry and Physics

Uncertainties of parameterized surface downward clear-sky shortwave and all-sky longwave radiation.

S. Gubler, S. Gruber, and R. S. Purves

University of Zurich, Department of Geography, Zurich, Switzerland

Correspondence to: S. Gubler (stefanie.gubler@geo.uzh.ch)

Received: 17 September 2011 – Published in Atmos. Chem. Phys. Discuss.: 31 January 2012
Revised: 8 May 2012 – Accepted: 22 May 2012 – Published: 8 June 2012

Abstract. As many environmental models rely on simulating the energy balance at the Earth's surface based on parameterized radiative fluxes, knowledge of the inherent model uncertainties is important. In this study we evaluate one parameterization of clear-sky direct, diffuse and global shortwave downward radiation (SDR) and diverse parameterizations of clear-sky and all-sky longwave downward radiation (LDR). In a first step, SDR is estimated based on measured input variables and estimated atmospheric parameters for hourly time steps during the years 1996 to 2008. Model behaviour is validated using the high quality measurements of six Alpine Surface Radiation Budget (ASRB) stations in Switzerland covering different elevations, and measurements of the Swiss Alpine Climate Radiation Monitoring network (SACRaM) in Payerne. In a next step, twelve clear-sky LDR parameterizations are calibrated using the ASRB measurements. One of the best performing parameterizations is elected to estimate all-sky LDR, where cloud transmissivity is estimated using measured and modeled global SDR during daytime. In a last step, the performance of several interpolation methods is evaluated to determine the cloud transmissivity in the night.

We show that clear-sky direct, diffuse and global SDR is adequately represented by the model when using measurements of the atmospheric parameters precipitable water and aerosol content at Payerne. If the atmospheric parameters are estimated and used as a fix value, the relative mean bias deviance (MBD) and the relative root mean squared deviance (RMSD) of the clear-sky global SDR scatter between between −2 and 5 %, and 7 and 13 % within the six locations. The small errors in clear-sky global SDR can be attributed to compensating effects of modeled direct and diffuse SDR since an overestimation of aerosol content in the atmosphere results in underestimating the direct, but overestimating the diffuse SDR. Calibration of LDR parameterizations to local conditions reduces MBD and RMSD strongly compared to using the published values of the parameters, resulting in relative MBD and RMSD of less than 5 % respectively 10 % for the best parameterizations. The best results to estimate cloud transmissivity during nighttime were obtained by linearly interpolating the average of the cloud transmissivity of the four hours of the preceeding afternoon and the following morning.

Model uncertainty can be caused by different errors such as code implementation, errors in input data and in estimated parameters, etc. The influence of the latter (errors in input data and model parameter uncertainty) on model outputs is determined using Monte Carlo. Model uncertainty is provided as the relative standard deviation σ_{rel} of the simulated frequency distributions of the model outputs. An optimistic estimate of the relative uncertainty σ_{rel} resulted in 10 % for the clear-sky direct, 30 % for diffuse, 3 % for global SDR, and 3 % for the fitted all-sky LDR.

1 Introduction

Downward shortwave (SDR) and longwave radiation (LDR) strongly control the energy budget at the Earth's surface. They drive processes such as photosynthesis and evapotranspiration, and are therefore of great importance in a variety of areas such as hydrological, agricultural (Cooter and Dhakhwa, 1996), and energy technology studies (Schillings, 2004). Especially in view of climate change, the modeling of environmental processes is important in temporal and spatial estimation of changes and rates of change, and to improve

the knowledge about the complex interactions between the atmosphere, the Earth surface and subsurface. In mountain areas, changes in the energy budget can already be observed at small distances due to the strong topographic variability.

Modeling energy fluxes and their uncertainties at the land surface is a key step in many model applications. A wide variety of models estimating SDR or LDR have been proposed in the literature, ranging from complex physical models using radiative transfer schemes and integrating aerosol and gaseous profiles of the atmosphere (e.g. LOWTRAN or MODTRAN) to empirical models based on relations between meteorological variables. For many applications, sophisticated models such as MODTRAN are inappropriate due to their complexity, required input data and computational effort. This study is based on the clear-sky broadband radiation model by Iqbal (1983, based on Bird and Hulstrom, 1980, 1981) and empirical parameterizations for clear- and all-sky LDR found in the literature (e.g. Brutsaert, 1975; Konzelmann et al., 1994; Pirazzini et al., 2000). The performance of many of these parameterizations has extensively been evaluated (e.g. Gueymard, 1993, 2003a,b, 2011; Crawford and Duchon, 1998; Battles et al., 2000; Pirazzini et al., 2000; Nimielä et al., 2001a,b), but sensitivity or uncertainty studies are rare in the literature (e.g. Gueymard, 2003b; Schillings, 2004; Badescu et al., 2012). Thus we focus on evaluating the Iqbal (1983) clear-sky SDR model and fitting the LDR parameterization to six locations at different elevations in Switzerland, and estimating model sensitivities and uncertainties due to different error sources.

The Iqbal (1983) model has been chosen since it has shown to reproduce SDR reasonably well under different climatic settings (Gueymard, 1993; Battles et al., 2000; Gueymard, 2003b). Furthermore, it has been frequently used in impact model applications (e.g. Corripio, 2002; Gruber, 2005; Machguth et al., 2008; Helbig et al., 2009) as well as other studies aiming at an optimal use of solar power, for example (Schillings, 2004). The Iqbal (1983) model assumes a homogeneous atmosphere and uses an isotropic view factor approach. Due to these simplifications, input is limited to a few quantities such as screen-level temperature (i.e. the temperature at the height of the measurement device, here 2 m above the ground), relative humidity and atmospheric pressure, and model parameters consist of the amount of ozone, aerosols and water vapor in the overlying atmosphere, among others, to determine the transmission respectively scattering of the solar rays. Under clear skies and non-polluted conditions, transmittance from ozone, precipitable water, aerosols, mixed gases and the Rayleigh transmittance cause most atmospheric attenuation (Gueymard, 2003a). In the past, these parameters could "not be easily determined from normally available information" (Dozier, 1980). Nowadays, ozone, aerosol content and water vapor is measured and can be obtained from Aeronet or satellite data such as MODIS for many locations, the datasets however often have spatial or temporal gaps (Gueymard, 2003a). Using this data therefore requires temporal interpolation and spatial extrapolation causing errors that are propagated into model outputs (Gueymard, 2003b). Practical model applications incorporating parameterizations of the downward radiation as a driving factor of other environmental processes are usually restricted to few input quantities such as the variables recorded at ordinary weather stations. Such impact models often treat parameters such as ozone, aerosol content and water vapor as constants (Longman et al., 2012). On one hand, this approach reduces the time and data management effort of a model user, on the other hand it introduces a considerable source of uncertainty and error into the model (Gueymard, 2003b; Badescu et al., 2012).

This study investigates the uncertainty of the Iqbal (1983) model due to uncertainties in inputs and the above mentioned simplifications concerning the estimated atmospheric parameters. A Monte Carlo based uncertainty analysis is performed based on previously determined input error and parameter probability distributions. The latter are determined using high quality measurements and/or established parameterizations of the correspondent parameter, while the input measurements are obtained from MeteoSwiss. In a next step, some of the most commonly used clear-sky LDR parameterizations are fitted to local conditions in Switzerland, resulting in the identification of the most appropriate parameterizations. For one of these parameterizations, the total output uncertainty is assessed based on input and parameter uncertainty similarly as discussed above. Clouds are one of the main LDR forcings. Since cloud cover is only rarely measured and measurements are error-prone, it is common to estimate the cloud transmissivity as the ratio of the measured and modeled clear-sky global SDR during daytime. During the night, when this approach is not feasible, cloud transmissivity is interpolated. In a last step, we therefore examine different cloud transmissivity interpolations, and propagate inherent uncertainties into all-sky LDR model outputs.

Thus, the aims of the present study are:

- to evaluate the clear-sky SDR model by Iqbal (1983) at six sites in Switzerland;
- to calibrate diverse clear- and all-sky LDR models and to assess the best all-sky parameterizations for impact modeling studies in Switzerland;
- to study the output of different interpolation techniques of the cloud transmissivity during nighttime; and
- to estimate the total output uncertainty of the clear-sky SDR model by Iqbal (1983) and one of the all-sky LDR models due to uncertainties in input variables and parameters.

All these steps are necessary to estimate the all-sky LDR and its associated uncertainties during day- and nighttime. To reach these aims, we firstly introduce the data and the parameters necessary in the study. In Sect. 3, the methods to assess

Table 1. Meta data of the MeteoSwiss stations. At each place, one ANETZ and one ASRB station is located.

Location	Abbreviation	Lat (deg N)	Long (deg E)	Ele [m]
Locarno-Monti	OTL	46.1726	8.7874	367
Payerne	PAY	46.8116	6.9424	490
Davos	DAV	46.8130	9.8435	1590
Cimetta	CIM	46.2010	8.7908	1672
Weissfluhjoch	WFJ	46.8333	9.8064	2690
Jungfraujoch	JUN	46.5474	7.9853	3580

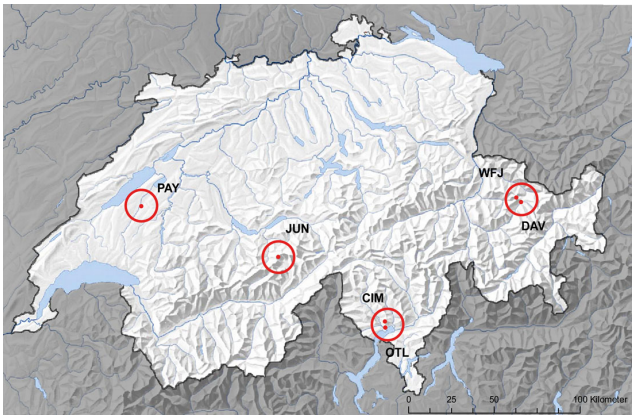

Fig. 1. Locations of the six MeteoSwiss stations in Switzerland (geodata © swisstopo). The coordinates of the locations are from MeteoSwiss (http://www.meteoswiss.admin.ch).

the sensitivity and the uncertainties in the clear-sky SDR and LDR model, and the validation and calibration methods are introduced. Then, the results are presented and discussed.

2 Data description

This modeling study is performed for six locations in Switzerland (Fig. 1, Table 1). The model is run with measurements from MeteoSwiss (Sect. 2.1) and estimated parameters (Sect. 2.2). The uncertainties in the input data and the parameters were assigned based on expert knowledge and literature, or were estimated based on representative measurements. Perceptual and structural model errors (cf., Beck, 1987; Beven, 1993; Kavetski et al., 2003; Gupta et al., 2005) are not investigated.

The data are structured as (a) input data, (b) physical and empirical model parameters and (c) validation data.

2.1 Input and validation data

The input data is obtained from the MeteoSwiss automatic meteorological network (ANETZ). The Alpine Surface Radiation Budget (ASRB, Philipona et al., 1996) network data serves for validation (SDR) and calibration (clear-sky and all-sky LDR). The number of study sites is restricted to the intersection of both networks. The study is performed with hourly data ranging from 1996 to 2008, resulting in 113 976 data points. Since synoptic cloud observations are rare (they exist only for 3 stations of this study) and error-prone, clear-sky hours are estimated according to the clear-sky index (CSI) introduced by Marty and Philipona (2000). The number of clear-sky hours varies between 25 000 and 38 000. The measurement errors are assumed to be normally distributed with zero mean. Standard deviations of the input and validation data (Table 2) were obtained from MeteoSwiss (courtesy of Rolf Philipona Philipona et al., 1995). All the measured data are denoted in equations with a superscript * (for example, T^* denotes measured air temperature).

2.2 Physical and empirical model parameters

2.2.1 SDR

The main focus of this study concerning modeled SDR lies on the estimation of the total output uncertainty of the Iqbal (1983) model due to the absorption, scattering and transmittance of the incoming solar radiation in the atmosphere, plus their reflection at the ground surface. Uncertainties in ozone column data, aerosol, precipitable water and in ground albedo are investigated and the probability density functions of each parameter are determined. Mean and standard deviation of the parameters are estimated using high quality measurements recorded in Switzerland, or using established parameterizations found in the literature. All uncertainty ranges are compared to estimates by Gueymard (2003b), and result to be representative. The uncertainty in Rayleigh and mixed gas transmittance is not investigated since it has limited influence on modeled SDR (Gueymard, 2003b).

Aerosol: Attenuation effects of scattering and absorption by aerosols were modeled according to Ångström (1929, 1930):

$$\tau_{\alpha\lambda} = \beta(\lambda/\lambda_0)^{-\alpha}, \quad (1)$$

where α is the wavelength exponent (also called Ångström exponent), β is the turbidity coefficient and $\lambda_0 = 1000\,\text{nm}$ for λ in nm. Aerosol optical depths (AOD) $\tau_{\alpha\lambda}$ data for diverse wavelengths λ are from aeronet.gsfc.nasa.gov. Level 2.0 AOD data for Davos for the years 2001 to 2010 were used in this study. The Ångström exponent α and the Ångström

Table 2. Input, model parameters and validation data with uncertainty distributions, mean μ and standard deviation σ. Note that the distribution for the ANETZ and ASRB measurements concern the error of the measurement (denoted with E), whereas the distribution in the parameters concerns the parameter value itself. Since ground albedo varies temporally and spatially, its distribution is estimated for each station and each month separately (Table B1).

	Measurement	Distribution	μ	σ	Unit	Symbol
Input	Air temperature	Normal (E)	0	0.2	K	T^*
	Relative humidity	Normal (E)	0	5	%	h_r^*
	Air pressure	Normal (E)	0	0.2	hPa	p^*
Parameter	Ozone column	Lognormal	314	38	DU	l
	Ångström exponent	Normal	1.38	0.46		α
	Ångström turbidity	Lognormal	0.039	0.05		β
	PrecWatConstant	Lognormal	47	0.38	g K cm^{-2} hPa^{-1}	a_w
	Ground Albedo	Lognormal				ρ_g
	Cloud transmissivity	Normal (E)	0	0.08		τ_c
Validation	Global SDR	Normal (E)	0	2 %	W m^{-2}	SDR^*_{glob}
	LDR	Normal (E)	0	2 %	W m^{-2}	LDR^*_{in}

turbidity coefficient β are determined from a linearised version of the Ångström's law in Eq. (1) (Gueymard, 2011):

$$\ln \tau_{\alpha\lambda} = \ln \beta - \alpha \ln(\lambda/\lambda_0). \quad (2)$$

To estimate α and β, we used $\tau_{\alpha\lambda}$ for wavelengths between 380 and 1020 nm. According to the resultant frequency distributions, α is assumed to be normally distributed with lower limit zero, and β is represented by a trimmed log-normal distribution with an upper limit equal to 0.5. The estimated mean value for α of 1.38 is close to the recommended value by Ångström (1930) $\alpha = 1.3$.

Water vapor: The effect of absorption due to water vapor contained in the atmosphere is estimated using the precipitable water w (Eq. A10). The precipitable water is the water contained in a column of unit cross section extending from the Earth's surface to the top of the atmosphere. Data of precipitable water is rarely available (Iqbal, 1983), and is thus often parameterized. Historical overviews of precipitable water parameterizations are given in Iqbal (1983) and Okulov et al. (2002). Here, the parameterization found in Reitan (1963); Leckner (1978) and Prata (1996) is used:

$$w = a_w \frac{h_r^* p_s}{T^*}, \quad (3)$$

where a_w is estimated (Eq. 4), h_r^* is the measured relative humidity in fractions of one, p_s is saturated water vapor pressure in hPa and T^* is screen-level temperature in K. The vapor pressure in saturated air is determined as a function of air temperature (Flatau et al., 1992). The parameter a_w [10g K hPa^{-1} cm^{-2}] is estimated as (Prata, 1996):

$$a_w = \frac{M_w}{R \cdot k \cdot \psi}, \quad (4)$$

where $M_w = 18.02\,\mathrm{g\,mol^{-1}}$ is the molecular weight of water vapor, $R = 8.314\,\mathrm{J\,K^{-1}\,mol^{-1}}$ is the universal gas constant and $\psi = 1.006$ is a constant. Further, $k = k_w + \frac{\gamma}{T^*}$, where $k_w = 0.44\,\mathrm{km^{-1}}$ is the inverse water vapor scale height (Reitan, 1963; Brutsaert, 1975) and γ is the lapse rate. The uncertainty of a_w is estimated by propagating the uncertainty inherent in the air temperature measurements and the lapse rate. The lapse rate is assumed to be normally distributed with mean equal to the standard value of $-6.5\,\mathrm{K\,km^{-1}}$ for the Alps and standard deviation of $1\,\mathrm{K\,km^{-1}}$, based on the investigations of Hebeler and Purves (2008). Following the investigations of Foster et al. (2006), a_w and w are assumed to be lognormally distributed. The uncertainty in a_w is around 1 %. By propagating the input measurement errors through Eq. 3, we observe an estimated uncertainty in precipitable water greater than 100 % (see Fig. 5), which is in accordance with Gueymard (2003b).

Ozone: MeteoSwiss provides accurate ozone column measurements in Arosa (Staehelin et al., 1998) on about two thirds of all days during the year. Ozone is assumed to be lognormally distributed. The estimated standard deviation of the ozone frequency distribution is around 12 % of the mean ozone, implying that the assumed uncertainty represents the ozone measurement uncertainty (5 to 30 %) as estimated by Gueymard (2003b) well.

Ground albedo: Ground albedo measurements for each of the study sites were obtained from the MODIS/Terra + Aqua BRDF and Calculated Albedo data set (ORNL DAAC, 2010). Ground albedo is assumed to be lognormally distributed (Oreopoulos and Davies, 1998; Mulrooney and Matney, 2007), with an upper cut-off at the maximum albedo. Due to the strong temporal and spatial variability of ground albedo, the measurements are separately examined for each study site and each month of the year (Table B1). Albedo is averaged over a square of 6.5 km by 6.5 km centered around each location.

Table 3. Parameterizations of clear-sky emissivity. p_v is the water vapor pressure [hPa], and T^* the measured temperature [K]. x_1, x_2 and x_3 denote the empirical parameters.

Publication	Abbr.	Eq.	ϵ_{cl}	x_1	x_2	x_3
Maykut and Church (1973)	may	18	x_1	0.7855		
Ångström (1915)	angs	8	$x_1 - x_2 \cdot 10^{-x_3 \cdot p_v}$	0.83	0.18	0.067
Brunt (1932)	brun	7	$x_1 + x_2 \cdot \sqrt{p_v}$	0.52	0.065	
Swinbank (1963)	swin	9	$x_1 \cdot T^{*2}$	9.365×10^{-6}		
Idso and Jackson (1969)	jack	10	$1 - x_1 \cdot \exp(-x_2 \cdot (273 - T^*)^2)$	0.261	7.77×10^{-4}	
Brutsaert (1975)	brut	12	$x_1 \cdot (\frac{p_v}{T^*})^{1/x_2}$	1.24	7	
Konzelmann et al. (1994)	konz	13	$0.23 + x_1 \cdot (\frac{100 p_v}{T^*})^{1/x_2}$	0.484	8	
Satterlund (1979)	satt	14	$x_1 \cdot (1 - \exp(-p_v^{\frac{T^*}{2016}}))$	1.08		
Idso (1981)	idso	11	$x_1 + x_2 \cdot p_v \cdot \exp(\frac{x_3}{T^*})$	0.7	5.95×10^{-5}	1500
Iziomon et al. (2003)	izio	16	$1 - x_1 \cdot \exp(-x_2 \cdot \frac{p_v}{T^*})$	0.43	11.5	
Prata (1996)	prat	15	$1 - (1 + 46.5 \cdot \frac{p_v}{T^*}) \cdot \exp(-(x_1 + x_2 \cdot 46.5 \cdot \frac{p_v}{T^*})^{x_3})$	1.2	3	0.5
Dilley and O'Brien (1997)	dill	17	$(x_1 + x_2 \cdot (\frac{T^*}{273.16})^6 + x_3 \cdot (\frac{46.5 \frac{p_v}{T^*}}{2.5})^{0.5})/(\sigma_{SB} T^{*4})$	59.38	113.7	96.96

2.2.2 LDR

The LDR parameterizations contain empirical parameters (Table 3) which originally were fitted to measurements at specific research sites (see Sect. 3.1.2 for details). In this study, we fit the selected parameterizations to the measurements at the six study sites in Switzerland, and identify reliable parameter values for the local conditions. The confindence intervals of the non-linear least-quares parameter estimation are used to quantify the uncertainty of the parameters. Clouds are a major forcing of LDR, and are estimated using measured and modeled global SDR. Uncertainties in modeled SDR thus are propagated to cloud transmissivity through Eq. (19). The standard deviation results in approximately 0.08 for modeled cloud transmissivity.

3 Methods

3.1 Model formulations

In this section, we give a brief overview of the model formulations and parameterizations used in the study.

3.1.1 Clear-sky SDR

In a first step, the clear-sky broadband global SDR is estimated (Iqbal, 1983, model C). For details the reader is asked to refer to Appendix A. The model estimates the direct SDR by calculating the radiation at the top of the atmosphere (Corripio, 2002), and the attenuation of the solar radiation by ozone, water vapor, aerosol and dry-air particles in the atmosphere. Then, the diffuse SDR due to Rayleigh-scattering, scattering by aerosols and the multiple reflection of the sun rays between the Earth's surface and the atmosphere is estimated. Direct and diffuse radiation sum up to the global SDR. Radiation due to scattering from surrounding terrain is included. However, it only accounts for a very small part of the total global SDR since the study locations are situated in locally flat terrain.

3.1.2 Clear-sky LDR

Clear-sky LDR is determined by the Stefan-Boltzmann law:

$$\mathrm{LDR_{cl}} = \epsilon_{atm} \cdot \sigma_{SB} \cdot T_{atm}^4, \quad (5)$$

where $\sigma_{SB} = 5.67 \times 10^{-8}\ \mathrm{W\,m^{-2}\,K^{-4}}$ denotes the Stefan-Boltzmann constant, ϵ_{atm} the bulk emissivity and T_{atm} the effective temperature of the overlying atmosphere. In practice, $\mathrm{LDR_{cl}}$ is estimated as:

$$\mathrm{LDR_{cl}} = \epsilon_{cl}(p_v, T^*) \cdot \sigma_{SB} \cdot T^{*4}, \quad (6)$$

where T^* denotes absolute air temperature (K) at the reference height of 2 m above the ground and ϵ_{cl} is the parameterized clear-sky emissivity. In the present study, twelve parameterizations (Table 3) are calibrated with measurements in Switzerland, and the most suitable ones are determined. The parameterizations are shortly presented in the following paragraph.

Estimating clear-sky emissivity based on water vapor pressure and temperature measurements has a long history. Brunt (1932) for example observed a linear relationship between ϵ_{cl} and $\sqrt{p_v}$. He showed that fitting a linear regression line:

$$\epsilon_{cl} = x_1 + x_2 \cdot \sqrt{p_v} \quad (7)$$

represented clear-sky emissivity better than the Ångström (1915) formula:

$$\epsilon_{\mathrm{cl}} = x_1 + x_2 \times 10^{-x_3 p_{\mathrm{v}}} \tag{8}$$

for measurements made in Uppsala (Asklöf, 1920). The parameter values for Brunt (1932) however vary significantly for different locations due to different rates of changes of air temperature and vapor pressure with elevation, but also due to differing methods estimating vapor pressure (Brunt, 1932). The parameters used here were estimated with monthly measurements from Benson, UK (Dines, 1921). Swinbank (1963) states that the relationship between ϵ_{cl} and p_{v} found by Ångström (1915) and Brunt (1932) basically arise from the relationship between humidity and temperature, and would only be appropriate for an atmosphere of constant grayness (e.g. Idso and Jackson, 1969). A better representation of $\mathrm{LDR_{cl}}$ was found using temperature alone (Swinbank, 1963):

$$\mathrm{LDR_{cl}} = x_1 \sigma_{SB} T^{*6}, \tag{9}$$

with $x_1 = 5.31 \times 10^{-13}$ in Australia, $x_1 = 5.21 \times 10^{-13}$ for the Benson measurements, and $\mathrm{LDR_{cl}}$ in $\mathrm{mWcm^{-2}}$. Idso and Jackson (1969) proposed the relation:

$$\epsilon_{\mathrm{cl}} = 1 - x_1 \exp(-x_2(273 - T^*)^2), \tag{10}$$

assuming that just above 273 K clear-sky emissivity may be described as an exponential function of temperature, and that the variation in ϵ_{cl} is symmetrical around the freezing point. They proved their relationship with $x_1 = 0.261$ and $x_2 = 7.77 \times 10^{-4}$ to provide more reliable results than Ångström (1915); Brunt (1932) and Swinbank (1963), and tested the parameterization for measurements in Alaska, Arizona, Australia and the Indian Ocean. Some years later, Idso (1981) established a physically based formula using new measurements of the total LDR for all wavelengths and the portions contained within the 10.5- to 12.5 µm and the 8 to 14 µm bands, resulting in:

$$\epsilon_{\mathrm{cl}} = x_1 + x_2 p_{\mathrm{v}} \exp(x_3/T^*) \tag{11}$$
$$x_1 = 0.7,\ x_2 = 5.95 \times 10^{-5},\ x_3 = 1500.$$

This is one of the first attempts to express the clear-sky effective emissivity in dependence of both temperature and water vapor. Earlier, Brutsaert (1975) suggested:

$$\epsilon_{\mathrm{cl}} = x_1 (\frac{p_{\mathrm{v}}}{T^*})^{1/x_2},\ x_1 = 1.24,\ x_2 = 7 \tag{12}$$

by integrating the Schwarzschild's radiative-transfer equation for simple atmospheric profiles. The formula can be reduced to $\epsilon_{\mathrm{cl}} = 0.553 p_{\mathrm{v}}^{1/7}$ for $T = 288$ K since it not very sensitive to changes in temperature (Brutsaert, 1975). To include the effect of greenhouse gases other than vapor pressure on LDR, Konzelmann et al. (1994) changed Brutsaert (1975) equation to:

$$\epsilon_{\mathrm{cl}} = 0.23 + x_1 (\frac{p_{\mathrm{v}}}{T^*})^{1/x_2}, \tag{13}$$

where $x_1 = 0.443$ and $x_2 = 8$ were optimal for measurements on the Greenland ice sheet. Note that p_{v} is in Pascal in the Konzelmann et al. (1994) publication. To be consistent, we use $\epsilon_{\mathrm{cl}} = 0.23 + x_1 (\frac{100 p_{\mathrm{v}}}{T^*})^{1/x_2}$ here. Another physically based equation taking into account both temperature and water vapor was proposed by Satterlund (1979) to ensure that ideal black body radiation is not exceeded by any extreme temperature or humidity value. Tested with measurements from Aase and Idso (1978) at Sidney, Montana, his formula resulted in:

$$\epsilon_{\mathrm{cl}} = x_1 \cdot (1 - \exp(-p_{\mathrm{v}}^{\frac{T^*}{2016}})),\ \text{where } x_1 = 1.08. \tag{14}$$

Prata (1996) found:

$$\epsilon_{\mathrm{cl}} = 1 - (1 + u)\exp(-(x_1 + x_2 u)^{x_3}), \tag{15}$$

with $u = 46.5 \frac{p_{\mathrm{v}}}{T^*}$ to represent the full long-wave spectrum such that $\epsilon_{\mathrm{cl}} \to 1 - \exp(-x_1^{x_3}) = \text{const}$ for $u \to 0$ and $\epsilon_{\mathrm{cl}} \to 1$ for $u \to \infty$. Prata (1996) estimated $x_1 = 1.2$, $x_2 = 3$ and $x_3 = 0.5$ for the measurements of Robinson (1947, 1950), the data that was also used by Brutsaert (1975). Iziomon et al. (2003) suggested another equation:

$$\epsilon_{\mathrm{cl}} = 1 - x_1 \exp(-x_2 \frac{p_{\mathrm{v}}}{T^*}),\ x_1 = 0.43 \text{ and } x_2 = 11.5 \tag{16}$$

which was fitted to measurements performed in Germany, whereas Dilley and O'Brien (1997) estimated $\mathrm{LDR_{cl}} = (1 - \exp(-1.66\tau))\sigma_{\mathrm{SB}} \cdot T^*$ where $\tau = 2.232 - 1.875(T/273.16) + 0.7356(w/2.5)^{1/2}$ is the grey-body optical thickness. His aim was to represent the main emission processes of the lower atmosphere, i.e. emission from water vapor and CO_2. Approximating the exponential by power series and neglecting all but the lowest order multinomials leads to:

$$\mathrm{LDR_{cl}} = x_1 + x_2 (T^*/273.16)^6 + x.3\sqrt{w/2.5}, \tag{17}$$
$$x_1 = 59.38,\ x_2 = 113.7,\ x_3 = 96.96.$$

The exponent of temperature is in accordance with the findings by Swinbank (1963). The simples equation assuming constant emissivity:

$$\epsilon_{\mathrm{cl}} = \text{const} \tag{18}$$

resulted convenient for Maykut and Church (1973) in Point Barrow, Alaska, and König-Langlo and Augstein (1994) for Arctic and Antarctic measurements.

3.1.3 Cloud transmissivity and cloud cover

The amount of clouds in the atmosphere determines the difference between clear-sky and all-sky LDR. Since cloud observations rarely exist, it is common to estimate the cloud

transmissivity τ_c as the ratio of the estimated clear-sky global SDR_{glob} and the measured global SDR^*_{glob} (e.g. Greuell et al., 1997):

$$\tau_c = \frac{SDR^*_{glob}}{SDR_{glob}}. \quad (19)$$

Note that $\tau_c < 1$ if the sky is overcast, and $\tau_c = 1$ denotes clear-sky conditions. Most parameterizations for all-sky LDR are based on the cloud-factor N, which is zero if the sky is completely clear, and one if the sky is cloud-covered. The linear relation between τ_c and N (Crawford and Duchon, 1998):

$$N = 1 - \tau_c \quad (20)$$

is used in this study. Different relationships involving a quadratic dependence of N and τ_c (Greuell et al., 1997) or even containing further parameters such as the relative humidity (Sicart et al., 2006) can be found in the literature.

3.1.4 All-sky LDR

Existing all-sky LDR parameterizations were summarized and tested for measurements recorded at Ny-Ålesund, Spitsbergen by Pirazzini et al. (2000) and result in the following two equations:

$$LDR_{all} = LDR_{cl} \cdot (1 + aN^{p_0}) \quad (21)$$

and

$$LDR_{all} = (\epsilon_{cl}(1 - N^{p_1}) + \epsilon_{oc}N^{p_2})\sigma_{SB}T^{*4}, \quad (22)$$

where ϵ_{cl} is the estimated clear-sky emissivity, a, p_0, p_1 and p_2 are parameters and ϵ_{oc} is the cloud emissivity. In this study, a slightly modified formula is further examined:

$$LDR_{all} = (\epsilon_{cl}\tau_c^{\tilde{p_1}} + \tilde{\epsilon}_{oc}(1 - \tau_c^{\tilde{p_2}}))\sigma_{SB}T^{*4}, \quad (23)$$

where the all-sky LDR is determined based on cloud transmissivity directly. This has the advantage of not having to choose a conversion from τ_c to N, but the disadvantage that a comparison with published values for the parameters $\tilde{p_1}$, $\tilde{p_2}$ and $\tilde{\epsilon}_{oc}$ is not possible.

3.1.5 Interpolation of cloud transmissivity during nighttime

The cloud transmissivity can, during daytime, be estimated according to Eq. 19. During the night, it is often determined by linearly interpolating between the last point in time at sunset, and the first point in time in the morning, or using a constant interpolation taking a mean cloud amount value from the preceding afternoon (Lhomme et al., 2007). These interpolated cloud transmissivity estimates are rarely validated due to the lack of available data. Here, we use different interpolation techniques, calculate the all-sky LDR during the night and evaluate the outputs with the ASRB measurements. The interpolation methods are:

1. linear interpolation between a mean value of x points in time (where each point in time represents an hourly value) before sunset and x points in time after sunrise,
2. constant interpolation of the mean value of x points in time before sunset,
3. constant interpolation of the mean value of x points in time after sunrise,

where $x = 1, 2, ..., 6$.

3.2 Model evaluation

The models are evaluated by a) investigating the model sensitivities to certain previously selected parameters, b) assessing the models' output uncertainty coming from uncertainty in input data and model parameters, c) comparing model outputs to measurements for validation, and d) calibrating diverse empirical and physical LDR parameterizations to conditions in Switzerland. To investigate a) and b), a probability density function (often called prior distribution, Table 2) is assigned to estimate the errors in the input variables and the parameters (Sect. 2.2). The errors in the parameters and input measurements are assumed to be independent. These distributions form the basis to analyze the local sensitivity of the model to each parameter (Sect. 3.2.1), and to perform a Monte Carlo based uncertainty analysis (Sect. 3.2.2). Using the mean parameter values and zero error for the input measurements, a simulation is run and the models are validated (Sect. 3.2.3). Calibration of the LDR parameterizations is performed based on non-linear least-squares estimation (Sect. 3.2.4).

3.2.1 Sensitivity analysis

SDR: Local relative sensitivities of direct, diffuse and global clear-sky SDR to ozone, precipitable water, the Ångström parameters and ground albedo are estimated. The sensitivities are estimated for constant path length $m_r = 2$, the path length estimated for a mean solar zenith angle of around 60 degrees at Jungfraujoch. Each model parameter θ_i is varied, unless the interval exceeds the physically possible values, within the interval $[\mu_i - 2\sigma_i, \mu_i + 2\sigma_i]$ while all other parameter $\theta_{j \neq i}$ are kept fixed at μ_j. Thereby, the influence of 97 % of the most plausible parameter values on SDR is investigated.

LDR: The sensitivity analysis focuses on the three main inputs determined in a preliminary analysis: cloud transmissivity, air temperature and relative humidity. LDR sensitivity is expressed as the *relative standard deviation* σ_{rel} of the output frequency distribution by varying the errors of each input variable according to its prior distribution, and keeping the others fixed. This is repeatedly done for different values of air temperature, relative humidity and cloud transmissivity to study the interactions between the three variables.

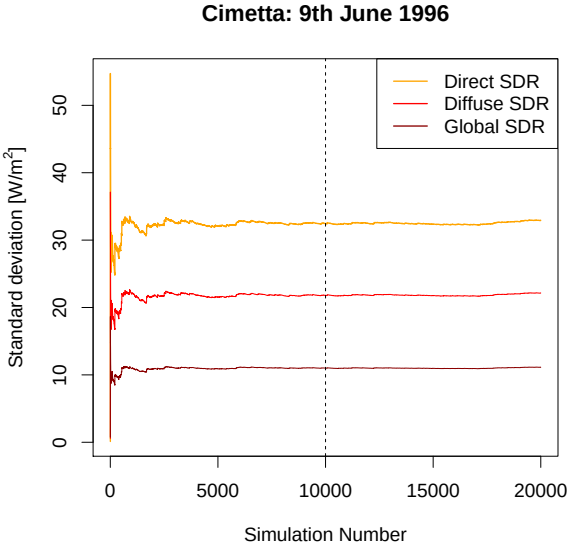

Fig. 2. Standard deviations of the model simulations at Cimetta. 10 000 model simulations result sufficient to reach stable standard deviations of the output frequency distribution.

3.2.2 Uncertainty assessment

Monte-Carlo based methods are widely used to derive the frequency density of the output of a model due to the simple implementation even for complex, non-linear models. 10 000 model simulations were sufficient to estimate total model output uncertainty (Fig. 2). The standard uncertainty of the model is defined as the standard deviation $\sigma_{t,\mathrm{abs}}$ of the model result at each time step (JCGM, 2008). The relative uncertainties are $\sigma_{t,\mathrm{rel}} := \sigma_{t,\mathrm{abs}}/\mu_t$. The 90 %-quantile and the median of the relative uncertainties for all time steps are estimated, and used as conservative respectively confidence estimates of the total output uncertainty. Further, a function $f(\mathrm{SDR}) = \sigma_{\mathrm{SDR,\,rel}}$ is fitted to the relative uncertainties using non-linear least-squares regression to derive the relative uncertainty in dependence of the modeled radiation.

3.2.3 Validation

Clear-sky global SDR and all-sky LDR are validated using the ASRB measurements (Sect. 2.1). The models are evaluated for a simulation which is performed with the measured input time series (assumed error-free) and the fixed parameter values μ (Table 2). According to Gueymard (2011), model performance is measured using the mean bias deviance (MBD) and the mean root squared deviance (RMSD) expressed in percent of the mean measured radiation. This naming is preferred over the often found mean bias error (ME) and root mean squared error (RMSE) to emphasize that a deviation between the model output and the measured value can come from both model error and measurement uncertainty (Gueymard, 2011). The MBD is a simple and very familiar measure that neglects the magnitude of the errors (i.e. positive errors can compensate for negative ones):

$$\mathrm{MBD} = \frac{1}{\overline{y^*}} \cdot \frac{\sum_{t=1}^{n} e_t}{n} \tag{24}$$

$$\mathrm{MBD} \in (-\infty, \infty),\ \mathrm{MBD}_{\mathrm{perf}} = 0,$$

where $e_t := y_t - y_t^*$ are the residuals of the models. Here, y_t denotes the modeled output variable, and y_t^* is the corresponding measured variable. The RMSD is:

$$\mathrm{RMSD} = \frac{1}{\overline{y^*}} \cdot \sqrt{\frac{1}{n}\sum_{t=1}^{n} e_t^2}, \tag{25}$$

$$\mathrm{RMSD} \in [0, \infty),\ \mathrm{RMSD}_{\mathrm{perf}} = 0.$$

It accounts for the average magnitude of the errors and puts weight on larger errors, but does not account for the direction of the errors. For clarity, both MBD and RMSD are expressed in percents throughout the manuscript. The correlation coefficient R measures the linear agreement between the modeled and the measured variable:

$$\mathrm{R} = \frac{\sum_{t=1}^{n}(y_t - \overline{y})(y_t^* - \overline{y^*})}{\sqrt{\sum_{t=1}^{n}(y_t - \overline{y})^2 (y_t^* - \overline{y^*})^2}} \tag{26}$$

$$\mathrm{R} \in [-1, 1],\ \mathrm{R}_{\mathrm{perf}} = 1,$$

The coefficient of determination R^2 indicates the amount of variation in one variable explained through the other.

3.2.4 LDR calibration using non-linear least-squares

Non-linear least-squares estimation (Bates and Watts, 1988; Bates and Chambers, 1992) is used to fit the clear-sky LDR parameterizations to observational data. In a first step, the clear-sky emissivity is estimated as:

$$\epsilon_{\mathrm{cl}} = \frac{\mathrm{LDR}^*_{\mathrm{in,cl}}}{\sigma_{\mathrm{SB}} T^{*4}}, \tag{27}$$

where both $\mathrm{LDR}^*_{\mathrm{in,cl}}$ and T^* are measurements of the ASRB stations. Then, the parameterizations presented in Table 3 are fitted to ϵ_{cl}. The start values for the non-linear estimation are the parameters presented in the respective publications. Thereby, optimal parameter values are obtained for each station. Furthermore, the parameterizations are fitted simultaneously to all stations, resulting in one single set of optimal parameters. Clear-sky situations are determined according to Marty and Philipona (2000); Dürr and Philipona (2004).

In a next step, the behaviour of the different parameterizations is evaluated according to three criteria: a) small MBD as an absolute value (Eq. 24), b) small RMSD (Eq. 25), and c) similarity in order of magnitude and sign of parameter estimates and published values. According to these criteria, the best parameterizations are identified.

4 Results

4.1 Clear-sky SDR

4.1.1 Validation

Modeled clear-sky global SDR is validated using the ASRB measurements. In general, a good linear agreement between model output and the measurements is observed (Fig. 3). The larger relative errors for low radiation can be attributed to the larger path length and thus higher influence of the estimated parameters ozone, precipitable water, aerosol content and ground albedo. Further, errors in cloud cover estimation by Marty and Philipona (2000); Dürr and Philipona (2004) might be responsible for some of the scatter observed at Jungfraujoch, for example (Fig. 3). To confirm the validity of the Iqbal-model for conditions in Switzerland, a model experiment was additionally performed using measurements of the atmospheric parameters (precipitable water, Ångström parameter α and β), and measured diffuse SDR in Payerne from the Swiss Alpine Climate Radiation Monitoring network (SACRaM) of MeteoSwiss. We see that the Iqbal (1983) model performs satisfactorily when using measured atmospheric parameters (Fig. 4, top). The scatter in diffuse SDR is normal for simple models such as the one by Iqbal (1983) (personal communication with C. Gueymard). Assuming that measurements of the atmospheric parameters do not exist, the diffuse SDR indicates large errors of $-17\,\%$ (MBD) and $37\,\%$ (RMSD) compared to $10\,\%$ (MBD) and $11\,\%$ (RMSD) when using the measurements (Fig. 4). Further, a limiting value of around $100\,\mathrm{W\,m^{-2}}$ in modeled diffuse SDR arises from an underestimation of the aerosol content. Global SDR however is modeled satisfyingly using constant values of the atmospheric parameters since the diffuse SDR only accounts for around one tenth of global SDR, and since errors due to "incorrect" aerosol content in direct and diffuse SDR are of opposite sign and compensate for each other (see Sect. 4.1.2).

To check for systematic errors, the residuals e_t were correlated with the input variables and the sun elevation. While for the input variables the correlations are low ($-0.2 < \mathrm{R} < 0.2$), errors slightly correlate with sun elevation (between 0 and 0.4 for direct, around -0.4 for diffuse and between -0.3 and 0.2 for global SDR). For direct SDR, the residuals scatter more (towards positive values) above the freezing point and for a relative humidity of around $60\,\%$, similarly the diffuse SDR (but in opposite direction). Due to compensating effects, this is not observed for global SDR. Since the correlations are not large, systematic errors are not further investigated.

One restriction already mentioned above must be kept in mind: clear-sky hours are based on the cloud estimation of Marty and Philipona (2000); Dürr and Philipona (2004) and thus error-prone. This might be a cause for some of the scatter in Fig. 3 at Jungfraujoch, for example. To analyze the effect of the clear-sky estimation, the validation measures were further estimated for clear-sky hours using synoptic cloud observations at the three stations Jungfraujoch, Payerne and Locarno-Monti. Since the overall picture of the model evaluation did not change the analysis strongly, the results of the clear-sky evaluation presented here are assumed to be reliable. A further indication of the validity of the approach is that the errors in the modeled clear-sky radiation do not correlate with the Dürr and Philipona (2004) cloud cover estimates.

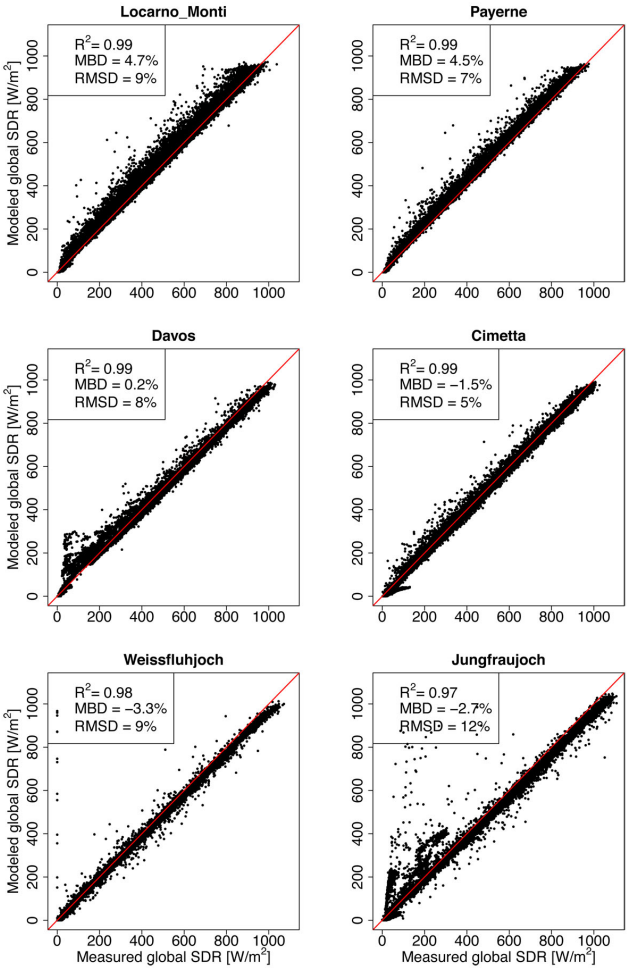

Fig. 3. Scatter plots of global modeled and measured SDR at all locations. The solid red line indicates the perfect fit.

4.1.2 Sensitivity of the clear-sky SDR

SDR is most sensitive to the atmospheric turbidity coefficient β (e.g. Gueymard, 2003b; Schillings, 2004, aerosol estimated from a visibility index), resulting in changes of -20 to $6\,\%$ for direct, -10 to $4\,\%$ global SDR, and of -30 to $80\,\%$ and more for diffuse SDR for $0 < \beta \leq 0.14$ for a mean path length of 2 (Fig. 5). The second most important parameter determining SDR is precipitable water, translating into an

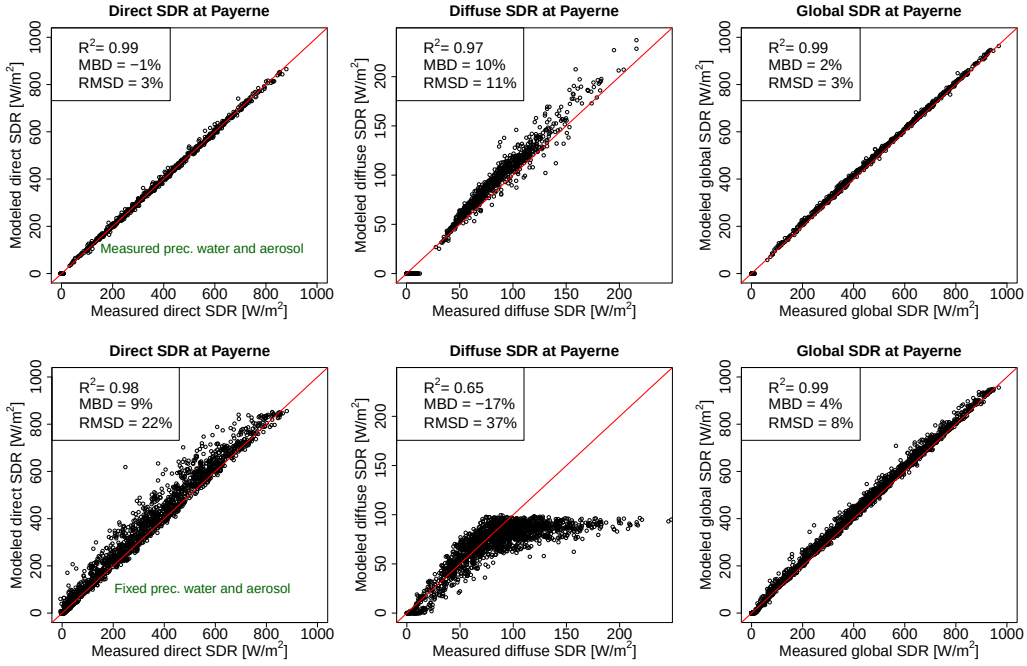

Fig. 4. Scatter plots of direct, diffuse and global SDR at Payerne. The top figures result from a model experiment when using measurements of the precipitable water and aerosol content. The lower figure show the model results when the atmospheric parameters have fixed values. The solid red line indicates the perfect fit.

uncertainty of around −4 to 10 % in direct and global SDR, whereas the Ångström coefficient α produces around −4 to 4 % uncertainty for direct, and a slightly smaller uncertainty for global SDR. Sensitivity to ozone is negligible for modeled SDR (less than 0.5 %). The ground albedo is an important parameter for diffuse SDR. It changes strongly within a year, having values of 0.1 for snow-free soils in summer, and more than 0.8 after fresh snow in winter. Clear-sky diffuse SDR changes by around ±20 % within this range of values. Since the diffuse SDR accounts only for a small part of the clear-sky global SDR, ground albedo does not play such an important role there (around ±2 %). The sensitivities in direct and diffuse SDR to aerosol content are opposite, i.e. an overestimation results in an underestimation of direct, but an overestimation of diffuse SDR. In the sum, these uncertainties compensate for each other and the relative error in global SDR is therefore smaller.

An additional uncertainty comes from estimating SDR at an hourly value for an instantaneous sun zenith angle. By calculating the solar zenith angle every 10 min and averaging the estimated SDR to hourly values, a mean deviance of less than 0.5 %, and a root mean squared deviance of 3 % was estimated for all direct, diffuse and global SDR.

4.1.3 Uncertainty of the clear-sky SDR

Uncertainty in direct SDR increases with decreasing elevation as there is a clear positive correlation of uncertainty with path length (Fig. 6), which can, to a smaller degree, also be observed for diffuse and global SDR. The 90 %-quantile of the absolute uncertainty for direct SDR goes from 43 W m^{-2} (JUN) to 55 W m^{-2} (OTL), and the median is around 38 W m^{-2}. Global SDR has the smallest absolute uncertainty of less than 20 W m^{-2}, resulting from the compensating effects of modeled direct and diffuse SDR with respect to aerosol content (see Sect. 4.1.2). The relative uncertainty for direct SDR approximates 5 % with increasing radiation. The median of direct SDR uncertainty does not exceed 10 % at all stations, however the 90 %-quantile of the relative uncertainties goes up to 20 %. For diffuse SDR, relative uncertainty goes from 25 % to 40 %, and the median scatters around 38 %. In contrast to direct and global SDR, the relative uncertainty increases with increasing diffuse SDR until around 60 W m^{-2}. For global SDR, the 90 %-quantiles of the relative uncertainty scatters around 6 % and goes down to 3 %. A conservative estimate (i.e. towards higher uncertainty) of the uncertainty in SDR is thus:

$$\mathrm{SDR}_i = \mathrm{SDR}_i^{\mathrm{est}} \cdot (1 + \varepsilon_{\mathrm{SDR}_i,\mathrm{rel}}), \tag{28}$$

$$\varepsilon_{\mathrm{SDR}_i,\mathrm{rel}} \sim \mathcal{N}(0, \sigma^2_{\mathrm{SDR}_i,\mathrm{rel}}),$$

with

$$\sigma_{\mathrm{SDR}_i,\mathrm{rel}} = \begin{cases} 0.2, & \text{if } i = \text{direct}, \\ 0.4, & \text{if } i = \text{diffuse}, \\ 0.06, & \text{if } i = \text{global}, \end{cases} \tag{29}$$

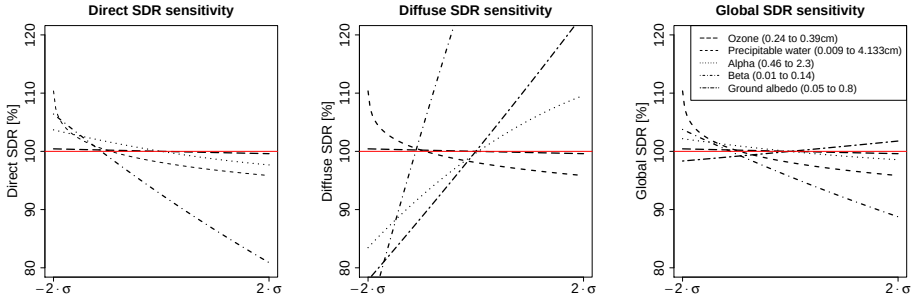

Fig. 5. Local sensitivities of clear-sky direct, diffuse and global SDR to ozone, precipitable water, the Ångström parameters α and β and ground albedo. The sensitivities are estimated for constant path length $m_r = 2$, the value for the mean solar zenith angle at Jungfraujoch. The range of the different parameters are given in the legend. The slope of the different curves reflect the relative sensitivity to each parameter. The mean downward radiation is indicated in red. The x-range is $\mu - 2\sigma$ to $\mu + 2\sigma$ avoiding parameter values without physical meaning (cf. Table 2).

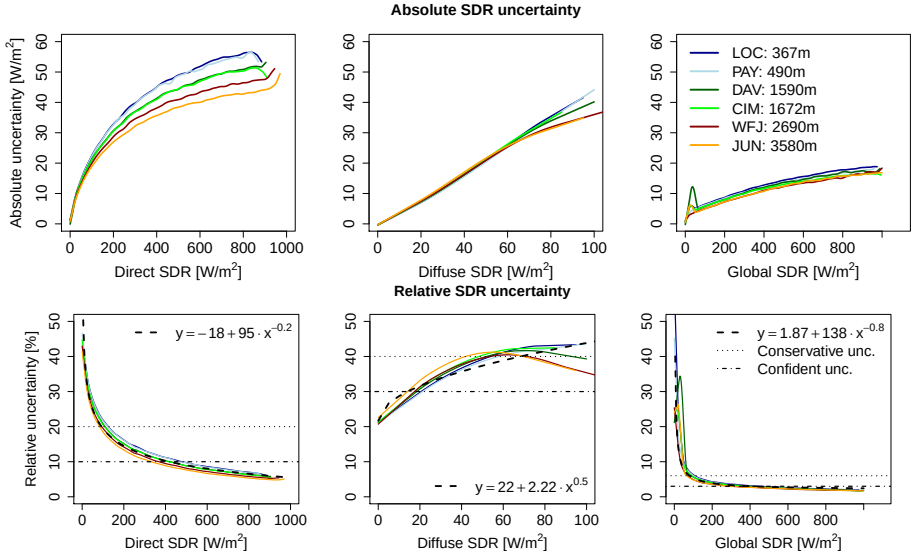

Fig. 6. Uncertainty expressed as smoothed mean lengths of the standard deviation of clear-sky direct, diffuse and global SDR, as a function of radiation [W m^{-2}]. The graphs were obtained by estimating the mean standard deviation of each 5 W m^{-2} radiation interval. Smoothing was performed using non-parametric regression. The dashed black line denotes the fit of the function $f(\mathrm{SDR}) = \sigma_{\mathrm{SDR,rel}}$, where $x := \mathrm{SDR}_i$ and $y := \sigma_{\mathrm{SDR}_i,\mathrm{rel}}$. The coefficients of the function $f(x) = y$ were obtained by non-linear least-squares regression.

while a more confident estimate results in:

$$\sigma_{\mathrm{SDR}_i,\mathrm{rel}} = \begin{cases} 0.1, & \text{if } i = \text{direct}, \\ 0.3, & \text{if } i = \text{diffuse}, \\ 0.03, & \text{if } i = \text{global}. \end{cases} \quad (30)$$

Further, a function $f(\mathrm{SDR}) = \sigma_{\mathrm{SDR,\,rel}}$ was fitted through the relative uncertainties for all three SDR types using non-linear least-squares estimation, resulting in:

$$\sigma_{\mathrm{SDR}_i,\mathrm{rel}} = \frac{1}{100} \begin{cases} -18 + \frac{95}{\mathrm{SDR}_i^{0.2}}, & \text{if } i = \text{direct}, \\ 22 + 2.22\sqrt{\mathrm{SDR}_i}, & \text{if } i = \text{diffuse}, \\ 1.87 + \frac{138}{\mathrm{SDR}_i^{0.8}}, & \text{if } i = \text{global} \end{cases} \quad (31)$$

where $\sigma_{\mathrm{SDR}_i,\mathrm{rel}}$ determines the standard deviation of the relative errors $\varepsilon_{\mathrm{SDR}_i,\mathrm{rel}}$ in modeled SDR. This function allows to determine the uncertainty in modeled clear-sky SDR more precisely for individual cases.

4.2 Clear- and all-sky LDR

4.2.1 Parameter estimation and validation of the clear-sky LDR

The non-linear least-squares fitting of the clear-sky LDR parameterizations (Table 3) to the six stations in Switzerland resulted in the parameter values presented in Table 4. For most parameterizations, a trend of the estimates is observed with elevation, indicating that a function depending on elevation

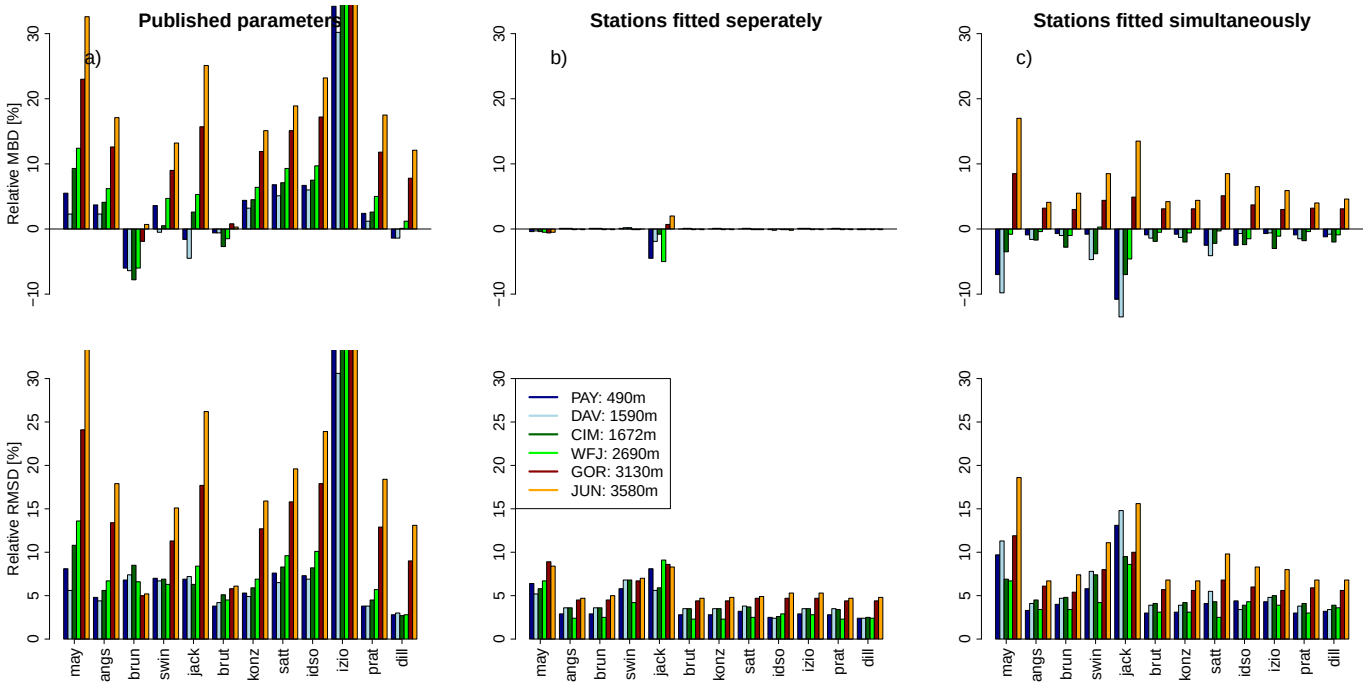

Fig. 7. MBD and RMSD for the LDR parameterizations using **(a)** the published parameter values, **(b)** the parameter values when fitting the parameterizations to each station separately and **(c)** when fitting all stations together simultaneously.

could result in an improvement of the parameterizations. For many applications, a modeler would apply the published parameterization as it is and use only one parameter value instead of modeling the elevation dependence of the parameter additionally. To get the best parameter estimate for all stations together, the parameterizations were also fitted to the measurements of all stations simultaneously (Table 4, second column). Except for Idso and Jackson (1969), all fitted parameters vary around the published values. The parameter in the exponential function of Idso and Jackson (1969) changes sign and thus appears to be not representative for high elevations such as JUN or WFJ. It is further less accurate than the other parameterizations together with the simple Maykut and Church (1973) parameterization (Fig. 7, middle and right). From the latter we conclude that clear-sky emissivity is not adequately represented by a constant value.

To compare the behaviour of the estimated parameters, the MBD and the RMSD of the clear-sky LDR of the published parameterizations were estimated in a first step (Fig. 7, left). The Brunt (1932); Brutsaert (1975) and Dilley and O'Brien (1997) have smallest MBD (-10 to 15 %) and RMSD (less than 10 % (except for Dilley and O'Brien (1997) at JUN and WFJ)). LDR is mostly overestimated by the models. In general (except for Brunt, 1932; Brutsaert, 1975), the lower elevation stations are better represented by the parameterizations. One possible reason is that most parameterizations were developed and fitted to measurements in lowland areas. Fitting the parameterizations to each location separately strongly improves model predictions leading to MBDs around zero and RMSDs of less than 10 % for all parameterizations (Fig. 7, middle). This can be expected since the parameterizations were trained and compared with and to the same data, i.e. validation was not performed on independent data. Measured air temperature and relative humidity used to *drive* the model are however *independent*; for fitting the ASRB and for validation the ANETZ measurements were used. When using the parameterizations with the simultaneously fitted parameter estimates (Fig. 7, right), the accuracy of the parameterization in comparison to the published values is also improved, and the uncertainty is reduced. Also in this experiment, training and validation data are not completely independent, the validation measurements in each case however consist only of one sixth of the training data. One can see that LDR at lower elevation stations is generally underestimated, and overestimated at the higher stations. The best performing parameterizations are Ångström (1915); Brunt (1932); Brutsaert (1975); Konzelmann et al. (1994) and Dilley and O'Brien (1997), having relative MBDs of less than 5 % and RMSDs of less than 10 %. We conclude that the behaviour of the parameterizations can be strongly improved by fitting them to local climatic conditions.

Since the performance of the best parameterizations is comparable, only one of the parameterizations was selected to study the all-sky situations. Konzelmann et al. (1994) was chosen because apparently the use of only two parameters is sufficient to model clear-sky emissivity in Switzerland. Further, the parameterization has earlier on been used in studies performed in Alpine regions (Greuell et al., 1997; Klok

Table 4. Values of the fitted parameters of the clear-sky LDR parameterizations to the six locations. The first column indicates the published parameter values and the second column indicates the estimated parameters when the stations are treated simultaneously.

	Pub	All	OTL	PAY	DAV	CIM	WFJ	JUN	
may_1	0.7855	0.69	0.74	0.77	0.72	0.70	0.63	0.59	
$angs_1$	0.83	0.79	0.83	0.86	0.80	0.77	0.72	0.65	
$angs_2$	0.18	0.26	0.21	0.19	0.17	0.19	0.20	0.18	
$angs_3$	0.067	0.10	0.05	0.03	0.06	0.09	0.14	0.31	
$brun_1$	0.52	0.53	0.60	0.64	0.60	0.58	0.51	0.48	
$brun_2$	0.065	0.073	0.049	0.042	0.050	0.055	0.075	0.084	
$swin_1$	9.365	8.97	9.05	9.43	9.34	8.94	8.58	8.27	$\times 10^{-6}$
$jack_1$	0.261	0.33	0.285	0.245	0.287	0.331	0.357	0.394	
$jack_2$	7.77	6.0	4.5	2.2	1.2	10.7	−4.5	−5.1	$\times 10^{-4}$
$brut_1$	1.24	1.12	1.05	1.03	1.00	1.00	1.00	0.96	
$brut_2$	7	8.6	10.46	11.62	12.22	11.54	10.33	10.73	
$konz_1$	0.484	0.43	0.45	0.46	0.46	0.44	0.41	0.39	
$konz_2$	8	5.7	7.19	8.09	8.27	7.71	6.52	6.54	
$satt_1$	1.08	1.00	1.01	1.03	1.01	0.99	0.94	0.91	
$idso_1$	0.7	0.57	0.64	0.63	0.61	0.62	0.55	0.53	
$idso_2$	5.95	0.48	0.503	0.08	0.06	3.30	1.946	4.012	$\times 10^{-5}$
$idso_3$	1500	2369	2239	2801	2913	1702	1967	1813	
$izio_1$	0.43	0.42	0.35	0.32	0.35	0.38	0.44	0.47	
$izio_2$	11.5	16.44	10.42	9.07	11.67	11.87	16.76	20.62	
$prat_1$	1.2	0.26	0.4	0.87	0.76	0.46	0.38	0.24	
$prat_2$	3	4.75	5.19	4.51	4.21	4.91	3.93	4.41	
$prat_3$	0.5	0.42	0.40	0.42	0.43	0.4	0.42	0.37	
$dill_1$	59.38	29.43	58.18	66.24	61.73	36.5	29.10	22.96	
$dill_2$	113.7	124.6	114.4	91.5	97.7	140.8	128.2	130.3	
$dill_3$	96.96	119.2	102.41	129.71	122.34	88.11	98.02	97.21	

Table 5. Fitted parameters of the all-sky LDR parameterizations presented in Eqs. 21, 22 and 23. The clear-sky emissivity is estimated according to Konzelmann et al. (1994). The second line consists of the estimates when all stations are fitted simultaneously, while the first indicates the values estimated by Pirazzini et al. (2000).

	Eq. (21)		Eq. (22)			Eq. (23)		
	a	p_0	ϵ_{oc}	p_1	p_2	$\tilde{\epsilon}_{oc}$	$\tilde{p}_1$	$\tilde{p}_2$
Published	0.40	2.00	0.979	6.00	4.00			
All	0.34	1.00	0.957	0.29	0.42	0.968	3.77	2.97
OTL	0.29	1.41	0.980	2.68	2.25	0.985	2.05	1.61
PAY	0.33	1.20	1.003	0.48	0.60	0.940	4.08	2.94
DAV	0.30	1.06	0.993	0.47	0.56	0.928	3.28	2.57
CIM	0.37	0.95	1.025	0.65	0.70	0.987	2.05	1.78
WFJ	0.46	0.74	1.028	0.27	0.37	0.926	5.02	3.74
JUN	0.50	0.61	0.988	1.21	0.82	0.828	0.76	1.24

and Oerlemans, 2002; Mittaz et al., 2002; Machguth et al., 2008). Konzelmann et al. (1994) is preferred over the Brutsaert (1975) parameterization due to the additive constant representing the clear-sky emissivity of a dry atmosphere to include the effect of greenhouse gases.

4.2.2 Parameter estimation and validation of the all-sky LDR during daytime

The parameterizations of all-sky LDR are based on an estimated clear-sky emissivity coupled with the effect of cloudiness or cloud emissivity. Clear-sky emissivity is estimated according to Konzelmann et al. (1994) with the fitted parameter estimates (Table 4, second column). The fitted values of the parameters of the two parameterizations (Pirazzini et al. (2000), Eqs. 21 and 22) and the modified parameterization

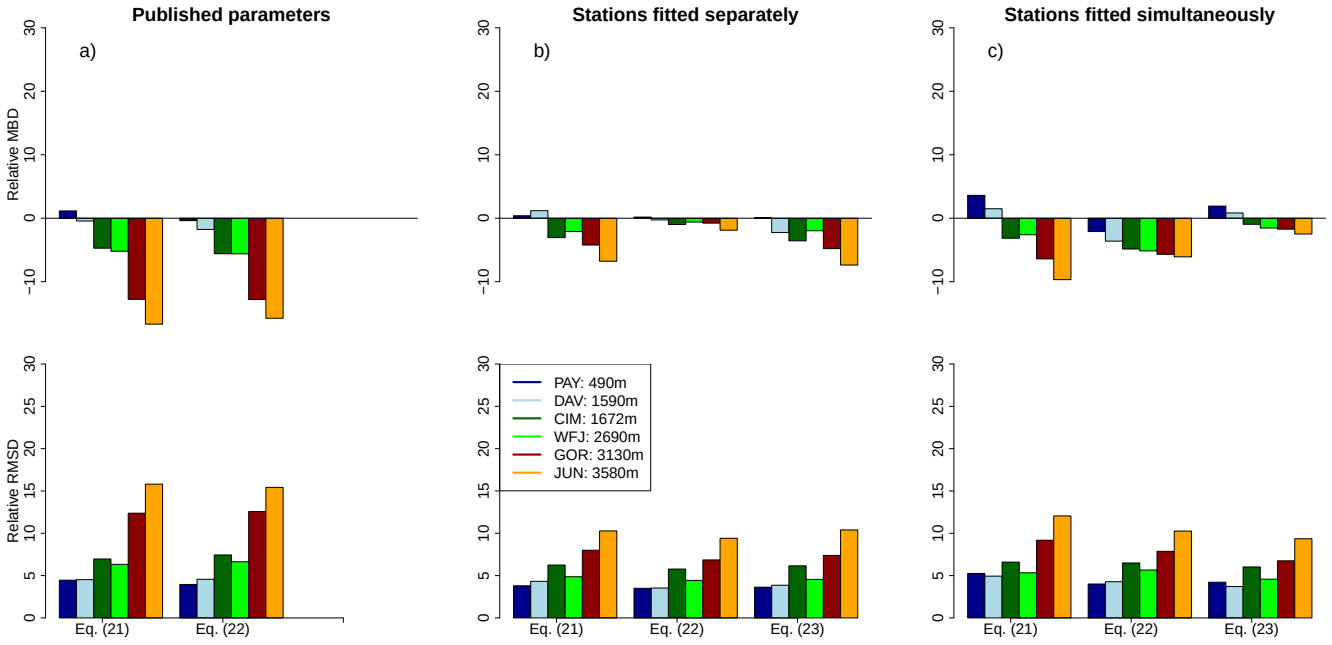

Fig. 8. MBD and RMSD for the LDR parameterizations using **(a)** the published parameter values by Pirazzini et al. (2000), **(b)** the parameter values when fitting the parameterizations to each station separately and **(c)** when fitting all stations together simultaneously. Clear-sky emissivity is estimated based on the Konzelmann et al. (1994) parameterization, using the parameters fitted for all stations simultaneously.

(Eq. 23) are presented in Table 5. The parameters reach values which are more or less comparable with those in the literature (Pirazzini et al., 2000, c.f. Table 3), however for CIM and WFJ, the estimated cloud emissivity ϵ_{oc} exceeds its physical range by being greater than 1. This problem does not arise for the modified parameterization (Eq. 23). MBD and RMSD are similar for all three parameterizations (Fig. 8), and slightly smaller for the modified version when fitting the stations simultanouesly. The relative MBD is less than 2 % for the latter, and RMSD is smaller than 10 %. Other than clear-sky LDR, all-sky LDR is overestimated at LOC and PAY, and underestimated at the higher elevation stations. The relative MBD and RMSD are comparable for clear-sky situations despite the greater uncertainties caused by cloud transmissivity. One reason for this is that LDR is around 30 to 50 $W\,m^{-2}$ greater for cloudy than for clear skies, and therefore the absolute MBD and RMSD are divided by a greater number. All-sky LDR deviates more strongly from the measurements than clear-sky LDR (Fig. 9).

We proceed with the modified parameterization Eq. (23) for two reasons: (a) conversion from cloud transmittance τ_c to cloud cover N is not necessary and (b) the fitting to the measurements resulted in physically reasonable cloud emissivity values.

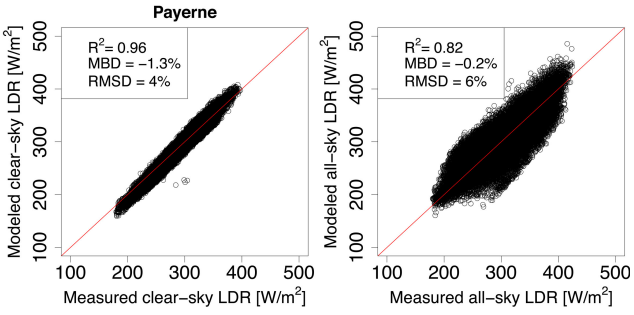

Fig. 9. Scatter plots of measured and modeled clear- and all-sky LDR according to Konzelmann et al. (1994) and Eq. 23.

4.2.3 Interpolation of cloud transmissivity during nighttime

The best all-sky LDR results during day- and nighttime were obtained by linearly interpolating the mean of the four cloud transmissivity values during the last hours in the afternoon preceeding the night, and the four hours in the following morning. For the simultaneous fitting, it resulted in a MBD of around 5 % and a RMSD up to 13 %, whereas the higher elevation stations have larger errors. Fitting the stations separately resulted in similar validation values. Constant interpolation resulted in errors that are around 2 % higher.

4.2.4 Sensitivity of the all-sky LDR

Modeled all-sky LDR (using Konzelmann et al. (1994) and Eq. 23) is sensitive to errors in air temperature, relative humidity and cloud transmissivity. The estimated parameters $x_1, x_2, \tilde{p_1}, \tilde{p_2}$ and $\tilde{\epsilon}_{\mathrm{oc}}$ have, within their estimated *confidence intervals*, only a minor influence. Cloud transmissivity has the greatest influence on LDR (Fig. 10). Modeled LDR changes up to around 15 % (standard deviation of around 7.5 %) on cold (−30 to −10° C) and slightly cloudy ($0.8 < \tau_c < 1$) days for $\varepsilon_{\tau_c} \sim \mathcal{N}(0, 0.08)$, whereas the uncertainty decreases for increasing air temperature to around 2 % (for air temperatures above 20 °C) (Fig. 10a). The sensitivity in LDR to cloud transmissivity decreases with increasing relative humidity, and is around 5 % for slightly cloudy skies (Fig. 10b). Changes in low cloud transmissivity (i.e. when the sky is overcast) only provoke a standard deviation of about 1% in simulated LDR. Accurate measuring or modeling of cloud transmissivity (or cloud cover) is therefore more important for slightly cloudy skies. In absolute values, an uncertainty of 0.08 in cloud transmissivity results in errors of around 4 (overcast) to 25 W m^{-2} (cold, high relative humidity, only few clouds). An error of 0.2 °C in measured air temperature causes a relative standard deviation of around 0.5% for clear-sky LDR, and around 0.3% in overcast situations (Fig. 10c). The sensitivity decreases for increasing temperature, and varies only slightly for differing humidities (Fig. 10d). The sensitivity to errors of 5 % in measured relative humidity increases to 3 % on clear-days, and to almost 0 % for overcast situations (Fig. 10f). With respect to air temperature, the sensitivity increases slightly with increasing temperatures, and ranges around 0.5 % (Fig. 10e).

4.2.5 Uncertainty of the all-sky LDR

The uncertainty of the all-sky LDR was estimated for the Konzelmann et al. (1994) clear-sky parameterization together with the all-sky parameterization in Eq. (23). The parameters were fitted to all stations simultaneously. The cloud transmissivity was linearly interpolated during nighttime according to Sect. 4.2.3. The uncertainty is estimated similarly to the uncertainty in SDR by doing a Monte Carlo simulation for all input variables, the cloud transmissivity and the fitted parameters.

The all-sky LDR output uncertainty is below around 14 W m^{-2} at all locations. In relative terms, the 90 %-quantile of the uncertainty is smaller than 6 % at all locations. The median of the relative uncertainty for the all-sky LDR is around 3 %. A conservative estimate of the uncertainty of the all-sky LDR is:

$$\mathrm{LDR_{all}} = \mathrm{LDR_{all}^{est}} \cdot (1 + \varepsilon_{\mathrm{LDR_{all,\,rel}}}), \quad (32)$$

$$\varepsilon_{\mathrm{LDR_{all,\,rel}}} \sim \mathcal{N}(0, \sigma^2_{\mathrm{LDR_{all,\,rel}}}),$$

with

$$\sigma_{\mathrm{LDR_{all,\,rel}}} = 0.06, \quad (33)$$

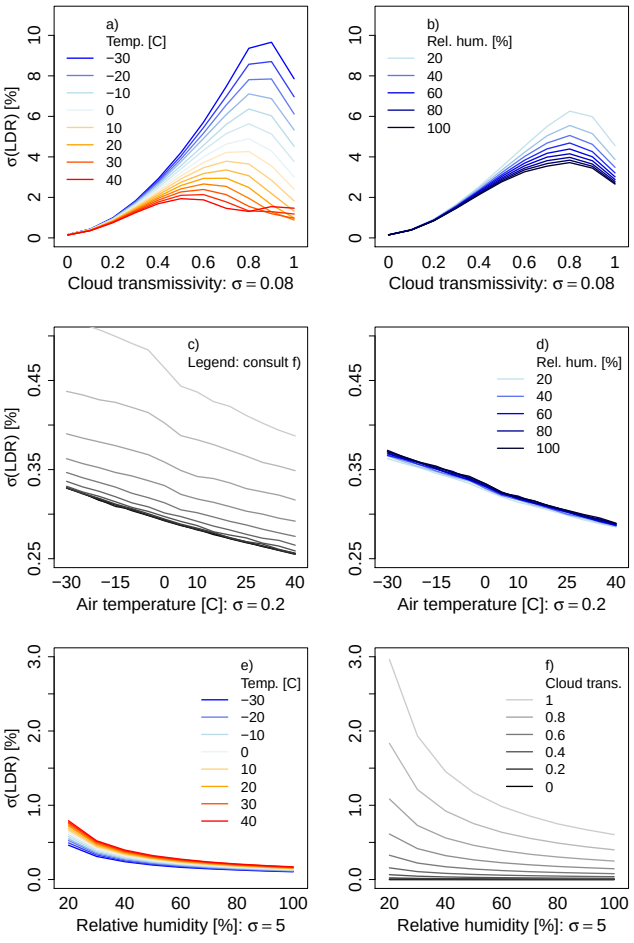

Fig. 10. LDR sensitivity to errors in estimated cloud transmissivity ($\sigma = 0.08$, **(a)** and **(b)**), measured air temperature ($\sigma = 0.2$ °C, **(c)** and **(d)**) and relative humidity ($\sigma = 5$ %, **(e)** and **(f)**). LDR sensitivity is expressed in the relative standard deviation of the simulated LDR using Monte Carlo. For air temperature for example, a mean value of 5 °C with an uncertainty of 0.2 °C results in a relative standard deviation of 0.45 % for clear-skies ($\tau_c = 1$) and 0.3% for overcast skies.

while the more confident estimate for the uncertainty in the LDR results in:

$$\sigma_{\mathrm{LDR_{all,\,rel}}} = 0.03. \quad (34)$$

The function $f(\mathrm{LDR_{all}}) = \sigma_{\mathrm{LDR_{all,\,rel}}}$ was fitted through the relative uncertainties of the LDR using non-linear least-squares estimation, which results in:

$$\sigma_{\mathrm{LDR_{all,\,rel}}} = \frac{1}{100} \frac{2681}{\mathrm{LDR_{all}^{1.21}}}, \quad (35)$$

where $\sigma_{\mathrm{LDR_{all,\,rel}}}$ is the standard deviation of the relative error $\varepsilon_{\mathrm{LDR_{all,\,rel}}}$.

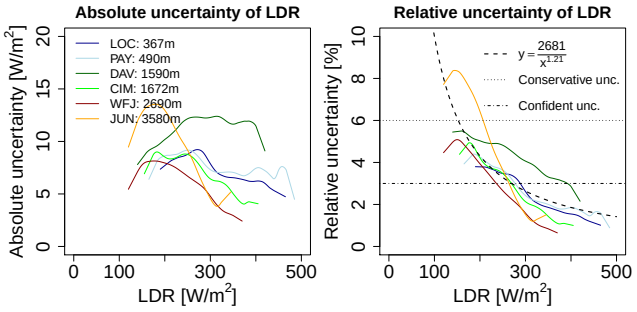

Fig. 11. Absolute and relative uncertainty of the modeled LDR. The clear-sky emissivity is estimated according to Konzelmann et al. (1994), and the all-sky parameterization is found in Eq. 23. The dashed black line denotes the fit of the function $f(\mathrm{LDR}) = \sigma_{\mathrm{LDR,\,rel}}$, where $x := \mathrm{LDR}$ and $y := \sigma_{\mathrm{LDR,\,rel}}$.

5 Discussion

The presented SDR and LDR models have been evaluated on many previous occasions (e.g. Gueymard, 1993, 2003b; Pirazzini et al., 2000; Klok and Oerlemans, 2002; Schillings, 2004; Sicart et al., 2006; Bilbao, 2006; Choi et al., 2008; Wang and Liang, 2009). The validation results for the clear-sky SDR and the all-sky LDR are in the range of these publications. We therefore only shortly comment our results with respect to some studies being of importance for the present study.

5.1 Evaluation of the clear-sky SDR model

According to Gueymard and Myers (2008), a clear-sky SDR model fits the measurements well if the MBD lies within ± 10 % and the RMSD< 20 % for global, and the MBD lies within ± 20 % and the RMSD<30 % for diffuse SDR. In Payerne, the Iqbal (1983) model C fulfills the even more stringent criteria by Badescu et al. (2012) (−5 % <MBD < +5 % and RMSD <15 % for global, and −10 % < MBD < +10 % and RMSD <30 % for diffuse SDR) if using measurements of the atmospheric variables in the model. In addition, the criteria are fulfilled for *global* SDR at all six stations even using *fixed* values of the atmospheric parameters. These findings are in agreement with Badescu et al. (2012) who tested the Iqbal (1983) model C together with 53 other clear-sky SDR models of diverse complexity on their performance and sensitivities in Cluy-Napoca and Bucharest, Romania. Badescu et al. (2012) however shows that the Iqbal (1983) model C for global SDR has some deficiencies in Cluy-Napoca for some of the sensitivity stages that were investigated. Model simulations of stage 11 for example, where measurements of precipitable water, ozone and ground albedo are assumed to be missing and therefore fixed (to values comparable to the ones used in this study), do not fulfill the quality criteria. However at Bucharest, global SDR is modeled well for most stages, being in agreement with the satisfying behaviour of the Iqbal (1983) model observed here. The diffuse SDR has greater problems when measurements of the atmospheric parameters are not available (Fig. 4, bottom and Badescu et al., 2012). A modeler with a special interest in diffuse SDR, but lacking measurements of the atmospheric parameters, is therefore recommended to use one of the well performing models as identified by Badescu et al. (2012) (e.g. ASHRAE2005 or King).

5.2 Calibration and evaluation of diverse clear- and all-sky LDR models

Wang and Liang (2009) resumed that the Brunt (1932) and Brutsaert (1975) are two of the best performing LDR parameterizations, which is in accordance with the findings of this study (and additionally Dilley and O'Brien, 1997). A very recent study (Marthews et al., 2012) shows that the Dilley and O'Brien (1997) clear-sky parameterization performs best for measurements in the tropics (Caxiuanã, Brasil), resulting in RMSD of between 12 and 22 $\mathrm{W\,m^{-2}}$. For the measurements in Switzerland, Brutsaert (1975) however performs better than Brunt (1932) and Dilley and O'Brien (1997) if applied with the published parameter values. Brunt (1932) underestimates LDR at the lower elevation stations, while Dilley and O'Brien (1997) overestimates LDR at the high elevation stations. When fitting the parameterizations to local conditions, the performance of Brunt (1932) and Brutsaert (1975); Dilley and O'Brien (1997) is similar, likewise the behaviour of some of the other parameterizations (Ångström, 1915; Konzelmann et al., 1994). This indicates that the key step for modeling LDR is not the selection of the parameterizations, but rather fitting the parameter values to local conditions, or using a parameterization developed or fitted at a place with comparable atmospheric conditions. This was also found by Bilbao (2006) who fitted the Brunt (1932); Swinbank (1963); Brutsaert (1975) and Idso (1981) parameterizations to measurements in central Spain.

Pirazzini et al. (2000) presented comparably high MBD and RMSD (MBD = −63 $\mathrm{W\,m^{-2}}$, RMSD = 64.5 $\mathrm{W\,m^{-2}}$) values using the Konzelmann et al. (1994) parameterization. We found that this is since Pirazzini et al. (2000) uses water vapor in Hectopascal instead of Pascal as originally published by Konzelmann et al. (1994). Using the correct unit for the water vapor, the Konzelmann et al. (1994) parameterizations performs acceptably (Fig. 7, left).

We have seen that transforming the estimated cloud transmissivity (Eq. 20) to cloud cover (Crawford and Duchon, 1998; Greuell et al., 1997; Sicart et al., 2006) to estimate all-sky LDR is not absolutely necessary (but does also provide reasonable results). By implementing the cloud transmissivity directly into the all-sky parameterization, errors from empirically estimated cloud conversions can be avoided. Similarly as for the clear-sky situation, fitting the parameterization to local conditions or using parameters estimated at similar locations is a crucial step to obtain reliable model

outputs. Wang and Liang (2009) validated the Brunt (1932) and Brutsaert (1975) parameterizations for all-sky conditions using $LDR_{all} = LDR_{cl} \cdot (1 - N) + N \cdot \sigma_{SB} \cdot T^{*4}$, where N is the cloud coverestimated from solar radiation according to Crawford and Duchon (1998). They found that all-sky LDR can be modeled with an average bias of 0.6 % and average standard deviation of 6 %, values which are comparable to the MBD and RMSD estimated in this study. The scatter of modeled clear-sky and all-sky LDR is large (Fig. 9), but seems to be in the order of other publications (Konzelmann et al., 1994; Crawford and Duchon, 1998; Wang and Liang, 2009).

5.3 Interpolation of cloud transmissivity during the night

The clear-sky index introduced by Marty and Philipona (2000) has the advantage to allow cloud detection during both day- and nighttime, in contrast to approaches using SDR. In contrast to global SDR, LDR is only rarely measured (cf. Alados-Arboledas et al., 1995; Wang and Liang, 2008) and needs often to be modeled to estimate the surface net radiation. The amount of clouds in the sky determines LDR, but cloud measurements are often error-prone and/or subjective. During daytime, cloud transmissivity is commonly estimated using modeled and measured global SDR (Greuell et al., 1997). We observed that during the night, linear interpolation using the mean cloud transmissivity estimated for the 4 to 6 hours of the preceeding afternoon and the following morning provided the best LDR estimates. Lhomme et al. (2007) used the mean cloud cover between 14 h and 16.30 h as a constant during the night, and observed errors in modeled LDR of around -7 $W m^{-2}$ (MBD) and 30 $W m^{-2}$ (RMSD) at the Andean Altiplano. In this study, we found that the constant interpolation provides around 2 % higher errors than linear interpolation.

5.4 Uncertainties of the clear-sky SDR and the all-sky LDR model

The validity of a clear-sky SDR model can be assessed using high quality and high sampling rate precipitable water and turbidity measurements, and great model performance can thereby be obtained. However, such measurements must often be inter- or extrapolated due to temporal or spatial incompleteness of the data source (Gueymard, 2003b). As mentioned above, a very detailed study investigating the sensitivity of 54 clear-sky SDR models on different sets of input data has only recently been published (Badescu et al., 2012), and determines models that behave satisfactorily even when not all the necessary input measurements are available. We think that it is worth to additionally quantify the error and the uncertainty that is thereby introduced as is presented in this study.

The energy in the atmosphere is a driving factor for any impact study concerned with the energy balance at the Earth's surface. Many impact models (Lehning et al., 2002; Klok and Oerlemans, 2002; Machguth et al., 2008) therefore incorporate SDR and LDR parameterizations. The downward radiation can be estimated and studied independently from any successive process at the Earth's surface and can be treated as an independent subsystem. A modeler dealing with model uncertainties can use the estimated uncertainties for the SDR (Eq. 28) and LDR (Eq. 32) by directly implementing them in his/her model, and propagating the uncertainties in SDR or LDR into the model output of interest. By direct implementing the presented uncertainty results, time and computational effort are reduced.

In accordance with earlier studies (Gueymard, 2003b; Schillings, 2004) we found that SDR is most sensitive to precipitable water and turbidity (Fig. 5). Errors in precipitable water can increase to 100 % due to atmospheric conditions or model discrepancies. The resultant uncertainty goes up to 10 % which is comparable to the errors of 2 to 15 % for direct SDR by Gueymard (2003b). Comparable results were also obtained for the direct SDR sensitivity to ozone, which are as low as 0.5 % for ozone (0.3 % for zenith angle zero degrees, and 1 % for zenith angle of 85° in Gueymard, 2003b). The greatest errors arise from variability in aerosols (−20 %). Sensitivity to nitrogen dioxide (NO_2) under polluted conditions is neglected since it is not explicitely modeled in Iqbal (1983), and since the NO_2 concentration in Switzerland is relatively low. In addition to the sensitivity in direct SDR, this study treats uncertainties of modeled diffuse and global SDR. We found that the sensitivity of direct and diffuse SDR to the Ångström parameters α and β are of opposite signs, and therefore compensate for each other when summed up to global SDR. *Modeled* global SDR is therefore *less uncertain* than would be expected after studying direct SDR alone. The confident total output uncertainty for global SDR is around 3 %, in comparison to 30 % uncertainty in diffuse and 10 % in direct SDR.

Concerning LDR, Sicart et al. (2006) found that clouds enhance LDR by around 16 % in Wolf Creek, Canada. On 90 % of the cloudy days, LDR increase was less than 30 %, and the maximal enhancement was found to be 50 %. Clouds thus predominantly determine LDR. We have shown that missing the correct cloud transmissivity value by around one tenth can result in differences of around 1 to 15 % in modeled LDR, in dependence of the atmospheric conditions. Therefore, accurate estimation or measuring the cloud cover or cloud transmissivity is of great importance to reduce errors in modeled LDR, especially when the sky is only partly cloudy.

We emphasize here that the presented uncertainties are in two ways subjective: (a) the selection of the parameters and input variables and (b) the prior distributions assigned to them. We tried to treat (a) and (b) as objectively as possible, however the reader should keep in mind that the assumptions influence the presented results.

6 Conclusions

The main findings of this study are shortly summarized:

- The Iqbal (1983) model reproduces clear-sky SDR well when using measurements of precipitable water and of the Ångström parameters α and β. Fixed atmospheric parameter values increase the errors in clear-sky global SDR from 2 % (MBD) and 3 % (RMSD) to around 5.5 % and 7 % at Payerne. The MBD and the RMSD of the clear-sky global SDR range from −3.3 to 5.5 % and from 2 to 12 % at the six locations, respectively, and therefore fulfill the quality criteria by Badescu et al. (2012). The Iqbal (1983) model is in a good linear agreement with measurements ($R^2 > 0.96$).

- The relative uncertainty for direct SDR is 10 %(20 %), for diffuse 30 %(40 %) and for global SDR 3 %(6 %) when estimating the relative uncertainty confidently (conservatively). In general, the uncertainty is greater for low sun elevations due to the larger path a sun ray traverses. The smaller relative uncertainty in clear-sky global SDR comes from the compensating effect of direct and diffuse SDR.

- The relative RMSD of the clear-sky LDR is less than 10 % for the best parameterizations (Dilley and O'Brien, 1997; Brutsaert, 1975; Konzelmann et al., 1994) and the MBD is around than 5 %. Fitting each location separately results in an elevation dependence of the parameters which could also be modeled in the future.

- Used with Konzelmann et al. (1994), the all-sky parameterization presented in Eq. 22 (Pirazzini et al., 2000) and similarly Eq. 23 perform best in order of MBD and RMSD, which are similar as for clear-skies. Conversion of cloud transmissivity to cloud cover is not necessary to estimate all-sky LDR.

- The study of the different interpolation techniques of the cloud transmissivity during nighttime has shown that a modeler preferably averages the cloud transmissivity estimated during 4 to 6 h before sunset and after sunrise and then linearly interpolates between the averages. This results in MBD of around 5 % and RMSD of 13 % for the resultant all-sky LDR.

- The output uncertainty of the all-sky LDR is less than 14 W m^{-2}, a conservative (confident) estimate of the relative uncertainty is 6 % (3 %). A trend with elevation is not observed.

- The key step when modeling LDR is not the selection of the parameterizations, but using a parameterization developed or fitted at a place with comparable atmospheric conditions.

7 Outlook

This study is focussed on the evaluation and uncertainty estimation of clear-sky SDR and all-sky LDR parameterizations at six locations in Switzerland due to unknown atmospheric parameters and errors in input data. Estimating the energy fluxes and their uncertainties at the place of potential input stations is certainly of value for further model applications in nearby locations. However, any model investigating the spatial distribution of a certain phenomenon comprises diverse formulae to extrapolate the measured input variables. The uncertainties due to these extrapolation techniques (such as the lapse rate for temperature) has not been studied. A further constraint of the presented study is the restriction to examine horizontal locations, neglecting thereby radiation from surrounding terrain and the topographical variability of model outputs. A study investigating these two issues would certainly deliver additional important information for further model applications.

Appendix A

Clear-sky global SDR

If not otherwise mentioned, all model formulations are from Iqbal (1983).

A1 Solar geometry

In a first step, the solar geometry for each location and time step is estimated according to the geometrical calculations by Corripio (2002). The eccentricity-corrected extraterrestrial solar radiation I_o is obtained by:

$$I_o = \rho \overline{I_o}, \tag{A1}$$

where $\rho \approx (\frac{r}{r_0})^2$, where r_0 is the actual and r the mean Sun–Earth distance, is an approximation of the relative distance traversed by the sun ray, and $\overline{I_o} = 1367\,\mathrm{W\,m^{-2}}$ is the solar constant. An approximation for ρ is (Spencer, 1971):

$$\begin{aligned}\rho =& 1.00011 + 0.034221\cos(\phi) + 0.00128\sin(\phi) \\ &+ 0.000719\cos(2\phi) + 0.000077\sin(2\phi),\end{aligned} \tag{A2}$$

where $\phi = 2\pi(d-1)/365$ is the day angle in radians and d is the day of the year.

A2 Direct radiation

The downward broadband SDR is given by

$$\mathrm{SDR_{dir}} = 0.9751 I_o \tau_r \tau_w \tau_o \tau_a \tau_g, \tag{A3}$$

where τ_r is the transmittance due to Rayleigh scattering, and τ_w, τ_o, τ_a and τ_g are the transmittances of water vapor, ozone,

aerosols and the uniformly mixed gases O_2 and CO_2, respectively. Attenuation due to dry air particles, aerosols and precipitable water is dependent on the length of the path a solar ray traverses before reaching the ground. Ignoring the Earth's curvature and under the assumption of a horizontal homogeneously distributed atmosphere the relative optical air mass m_r can be estimated as:

$$m_r = \frac{1}{\cos\Theta_Z}, \tag{A4}$$

where Θ_Z is the solar zenith angle. Attenuation increases with increasing zenith angle. Kasten (1966) developed an accurate estimation of the relative optical mass m_r considering the Earth's curvature and the refraction of the real atmosphere:

$$m_r = \frac{1}{cos\Theta_Z + 0.15(93.885 - \Theta_Z)^{-1.253}}. \tag{A5}$$

For non-standard pressures deviating from 1013.25 hPa at sea level, induced by weather or topography, the relative optical air mass m_r is modified to local condition air mass m_a:

$$m_a = m_r \frac{p^*}{1013.25}, \tag{A6}$$

where p^* is screen-level atmospheric pressure (hPa). Rayleigh scattering transmittance is:

$$\tau_r = \exp[-0.0903 m_a^{0.84}(1.0 + m_a - m_a^{1.01})]. \tag{A7}$$

Transmittance by ozone is given by:

$$\tau_o = 1.0 - [0.1611U_1(1.0 + 139.48U_1)^{-0.3035} - 0.002715U_1(1.0 + 0.044U_1 + 0.0003U_1^2)^{-1}], \tag{A8}$$

where $U_1 = lm_r$ is the ozone relative optical path length, and l is the ozone column in cm. The transmittance by uniformly mixed gases is given by:

$$\tau_g = \exp[-0.0127 m_a^{0.26}], \tag{A9}$$

and the transmittance of water vapor is obtained from:

$$\tau_w = 1 - 2.4959U_2[(1.0 + 79.034U_2)^{0.6828} + 6.385U_2]^{-1}. \tag{A10}$$

Here, $U_2 = wm_r$ is the pressure-corrected relative optical path length of precipitable water. The parameter w denotes the precipitable water (cm). Aerosol transmittance is parameterized as proposed in Iqbal's model A:

$$\tau_a = (0.12445\alpha - 0.0162) + (1.003 - 0.125\alpha) \cdot \exp(-m_a\beta(1.089\alpha + 0.5123)),\ \beta < 0.5, \tag{A11}$$

where α is known as the Ångström parameter and β is the Ångström turbidity parameter.

A3 Diffuse radiation

Diffuse radiation is estimated as the sum of the Rayleigh-scattered, the aerosol-scattered and the multiple reflected irradiance, i.e.:

$$SDR_{dif} = SDR_{dif,r} + SDR_{dif,a} + SDR_{dif,rfl}. \tag{A12}$$

The Rayleigh-scattered diffuse irradiance is estimated as:

$$SDR_{dif,r} = 0.79 I_o \cos\Theta_z \frac{\tau_o \tau_g \tau_w \tau_{aa} 0.5(1 - \tau_r)}{1 - m_a + m_a^{1.02}}, \tag{A13}$$

where τ_{aa} is the estimated transmittance of direct radiation due to aerosol absorptance:

$$\tau_{aa} = 1 - (1 - \omega_0)(1 - m_a + m_a^{1.06})(1 - \tau_a), \tag{A14}$$

where ω_0 is the single-scattering albedo. We set $\omega_0 = 0.9$ (Bird and Hulstrom, 1980). Diffuse irradiance due to scatttering of aerosols is:

$$SDR_{dif,a} = 0.79 I_o \cos\Theta_z \frac{\tau_o \tau_g \tau_w \tau_{aa} 0.84(1 - \tau_{as})}{1 - m_a + m_a^{1.02}}, \tag{A15}$$

where $\tau_{as} = \tau_a / \tau_{aa}$ is the fraction of the incident energy transmitted after scattering effects of aerosols. The between the Earth and the atmosphere multiply-reflected irradiance is:

$$SDR_{dif,rfl} = \frac{(SDR_{dir}\cos\Theta_z + SDR_{dif,r} + SDR_{dif,a})\rho_g\rho_a}{1 - \rho_g\rho_a}. \tag{A16}$$

The parameters ρ_g and ρ_a are ground albedo and albedo of the cloudless sky, respectively. The albedo of the cloudless sky is computed as:

$$\rho_a = 0.0685 + 0.16(1 - \tau_{as}). \tag{A17}$$

A4 Terrain reflected radiation

The terrain reflection radiation is estimated according to Dozier and Frew (1990):

$$SDR_{ter} = \rho_g \cdot (\frac{1 + \cos(slope)}{2} - svf) \cdot (SDR_{dir} + SDR_{dif}), \tag{A18}$$

where slope denotes the slope of the simulation point, and svf is the fraction of the sky visible at the simulation point. Since $\cos(slope) = \cos(0) = 1$ and the svf is large (between 0.97 and 1) for all simulation points, the terrain reflected radiation accounts only for a very small part of the global radiation.

A5 Global radiation

Global SDR is the sum of direct SDR (Sect. A2), diffuse radiation (Sect. A3) and the radiation reflected at surrounding terrain (Sect. A4), i.e. $SDR_{glob} = SDR_{dir} + SDR_{dif} + SDR_{ter}$.

Table B1. Mean and standarddeviation ($\mu|\sigma$) of the ground albedo from the MODIS/Terra+Aqua BRDF and Calculated Albedo data set, estimated at each location for a surrounding terrain of approximately 6.5^2 km^2 for each month of the year.

Month	CIM	DAV	GOR	JUN	OTL	PAY	WFJ
Jan	0.20|0.13	0.39|0.19	0.29|0.20	0.16|0.09	0.11|0.07	0.20|0.13	0.50|0.15
Feb	0.16|0.10	0.43|0.19	0.51|0.21	0.30|0.19	0.11|0.05	0.16|0.06	0.64|0.13
Mar	0.13|0.06	0.42|0.18	0.57|0.11	0.50|0.19	0.10|0.04	0.15|0.01	0.63|0.12
Apr	0.12|0.02	0.33|0.19	0.54|0.11	0.36|0.15	0.10|0.04	0.17|0.01	0.54|0.15
May	0.13|0.01	0.15|0.09	0.30|0.16	0.30|0.12	0.11|0.04	0.17|0.01	0.31|0.19
Jun	0.14|0.01	0.12|0.03	0.18|0.06	0.27|0.10	0.11|0.04	0.16|0.01	0.16|0.04
Jul	0.13|0.01	0.11|0.02	0.15|0.04	0.26|0.11	0.11|0.04	0.16|0.01	0.14|0.02
Aug	0.13|0.02	0.11|0.02	0.14|0.04	0.24|0.11	0.11|0.04	0.16|0.01	0.14|0.02
Sep	0.13|0.02	0.12|0.07	0.15|0.06	0.20|0.10	0.11|0.04	0.16|0.01	0.17|0.11
Oct	0.13|0.03	0.16|0.14	0.17|0.10	0.17|0.11	0.11|0.04	0.15|0.01	0.24|0.19
Nov	0.14|0.07	0.28|0.20	0.20|0.15	0.16|0.12	0.11|0.05	0.14|0.04	0.45|0.20
Dec	0.19|0.13	0.35|0.18	0.16|0.08	0.12|0.06	0.11|0.06	0.15|0.09	0.55|0.16

Appendix B

Estimated ground albedo distributions

The distribution of the ground albedo distribution for each station and each month of the year were estimated according to data from the MODIS/Terra+Aqua BRDF and Calculated Albedo dataset[1] (Table B1).

Acknowledgements. The authors are grateful to R. Philipona and L. Vuilleumier from MeteoSwiss for providing the high quality SACRaM and ASRB data together with the information about measurement uncertainty. We thank S. Endrizzi for extensive discussions about modeling the energy fluxes, and C. Gueymard for giving great advise and answering many questions. Comments from two anonymous reviewers helped to strongly improve the present manuscript. This study was funded by the Swiss National Science Foundation (SNSF) via the NCCR MICS project PermaSense, and further supported by X-Sense, funded through www.nano-tera.ch. All computational and statistical analyses were performed with R (www.cran.r-project.org).

Edited by: P. Monks

References

Aase, J. K. and Idso, S. B.: A comparison of two formula types for calculating long-wave radiation from the atmosphere, Water Resour. Res., 14, 623–625, 1978.

Alados-Arboledas, L., Vida, J. and Olmo, F. J.: The estimation of thermal atmospheric radiation under cloudy conditions, Int. J. Climatol., 15, 107–116, 1995.

Andreas, E. L. and Ackley, S. F.: On the differences in ablation seasons of Arctic and Antarctic sea ice-sheet, J. Atmos. Sci., 39, 440–447, 1982.

Ångström, A.: A study of the radiation of the atmosphere, Smithsonian Miscellaneous Collection, 65, 1–159, 1915.

Ångström, A.: On the atmospheric transmission of sun radiation and on dust in the air, Geografiska Annaler, 11, 156–166, 1929.

Ångström, A.: On the atmospheric transmission of sun radiation, Geografiska Annaler, 12, 130–159, 1930.

Asklöf, S.: Über den Zusammenhang zwischen der nächtlichen Wärmeaustrahlung, der Bewölkung und der Wolkenart, Geografiska Annaler, 2, 253–259, 1920.

Badescu, V., Gueymard, C., Cheval, S., Oprea, C., Baciu, M., Dumitrescu, A., Iacobescu, F., Milos, I. and Rada, C.: Computing global and diffuse solar hourly irradiation on clear sky. Review and testing of 54 models, Renew. Sustain. Energ. Rev., 16, 1636–1656, 2012.

Bates, D. M. and Chambers, J. M.: Nonlinear models, Chap. 10, Wadsworth and Brooks/Cole, Pacific Grove, CA, USA, 1992.

Bates, D. M. and Watts, D. G.: Nonlinear regression analysis and its applications, Wiley, New York, USA, 1988.

Battles, F. J., Olmo, F. J., Tovar, J. and Alados-Arboledas, L.: Comparison of cloudless sky parameterizations of solar irradiance at various Spanish midlatitude locations, Theor. Appl. Climatol., 66, 81–93, 2000.

Beck, M. B.: Water quality modeling: a review of the analysis of uncertainty, Water Resour. Res., 23, 1393–1442, 1987.

Beven, K.: Prophecy, reality and uncertainty in distributed hydrological modelling, Adv. Water Resour., 16, 41–51, 1993.

Bilbao, J. and de Miguel, A. H.: Estimation of daylight downward longwave atmospheric irradiance under clear-sky and all-sky conditions, J. Appl. Meteorol. Climatol., 46, 878–889, 2006.

Bird, R. E. and Hulstrom, R. L.: Direct insolation models, Tech. Report, Solar Energy Research Institute, Colorado, USA, 1980.

Bird, R. E. and Hulstrom, R. L.: Simplified clear sky model for direct and diffuse insolation horizontal surfaces, Solar Energy Research Institute, Colorado, USA, 1981.

Brunt, D.: Notes on radiation in the atmosphere, Q. J. Roy. Meteorol. Soc., 58, 389–420, 1932.

[1]MODIS download information for Cimetta: Product: MCD43A Location Centered on: Latitude [46.201], Longitude [8.7908] Size: Approximately 6.5 km wide and 6.5 km high time Period: 18 February 2000 to 20 July 2010 Selected Solar Zenith Angle is local Selected Optical Depth is 0.2

Brutsaert, W.: On a derivable formula for long-wave radiation from clear skies, Water Resour. Res., 11, 742–744, 1975.

Choi, M., Jacobs, J. M. and Kustas, W. P.: Assessment of clear and cloudy sky parameterizations for daily downwelling longwave radiation over different land surfaces in Florida, USA, Geophys. Res. Lett., 35, L20402, doi:10.1029/2008GL035731, 2008.

Cooter, E. and Dhakhwa, G.: A solar radiation model for use in biological applications in the South and Southeastern USA, Agric. Forest Meteorol., 79, 31–51, 1996.

Corripio, J. G.: Vectorial algebra algorithms for calculating terrain parameters from DEMs and solar radiation modelling in mountainous terrain, Geogr. Inf. Sci., 17, 1–23, 2002.

Crawford, T. M. and Duchon, C. E.: An improved parameterization for estimating effective atmospheric emissivity for use in calculating daytime downwelling longwave radiation, J. Appl. Meteorol., 38, 474–480, 1998.

Dilley, A. C. and O'Brien, D. M.: Estimating downward clear sky long-wave irradiance at the surface from screen temperature and precipitable water, Q. J. Roy. Meteorol. Soc., 124a, 1391–1401, 1997.

Dines, W. H.: Observations on radiation from the sky, and an attempt to determine the atmospheric constant of radiation, Meteorological Observations, Geophys. Mem., 18, 1921.

Dozier, J.: A clear-sky spectral solar radiation model for snow-covered mountainous terrain, Water Resour. Res., 16, 709–718, 1980.

Dozier, J. and Frew, J.: Rapid calculation of terrain parameters for radiation modeling from digital elevation data, IEEE T. Geosci. Remote, 28, 963–969, 1990.

Dürr, B. and Philipona, R.: Automatic cloud amount detection by surface longwave downward radiation measurements, J. Geophys. Res., 109, D05201, doi:10.1029/2003JD004182, 2004.

Efimova, N. A.: On methods of calculating monthly values of net long-wave radiation, Meteor. Gidrol., 10, 28–33, 1961.

Flatau, P. J., Walko, R. L., and Cotton, W. R.: Polynomial fits to saturation vapor pressure, J. Appl. Meteorol., 31, 1507–1513, 1992.

Foster, J., Bevis, M., and Raymond, W.: Precipitable water and the lognormal distribution, J. Geophys. Res., 111, D15102, doi:10.1029/2005JD006731, 2006.

Fung, I. Y., Harrison, D. E., and Lacis, A. A.: On the variability of the net longwave radiation at the ocean surface, Rev. Geophys. Space Phys., 22, 177–193, 1984.

Greuell, W., Knap, W. H., and Smeets, P. C.: Elevational changes in meteorological variables along a midlatitude glacier during summer, J. Geophys. Res., 102, 941–954, 1997.

Gruber, S.: Mountain permafrost: Transient spatial modelling, model verification and the use of remote sensing, Ph.D. Thesis, University of Zurich, Zurich, Switzerland, 2005.

Gueymard, C.: Critical analysis and performance assessment of clear sky solar irradiance models using theoretical and measured data, Sol. Energy, 51, 121–138, 1993.

Gueymard, C.: Direct solar transmittance and irradiance predictions with broadband models. Part I: detailed theoretical performance assessment, Solar Energy, 74, 355–379, 2003a.

Gueymard, C.: Direct solar transmittance and irradiance predictions with broadband models: Part II: validation with high-quality measurements, Sol. Energy, 74, 381–395, 2003b.

Gueymard, C. and Myers, D. R.: Validation and ranking methodologies for solar radiation models, In: Badescu, V. (Ed.), Modeling solar radiation at the earth surface, Berlin, Springer, 20, 479–509, 2008.

Gueymard, C.: Clear-sky irradiance predictions for solar resource mapping and large-scale applications: Improved validation methodology and detailed performance analysis of 18 broadband radiative models, Sol. Energy, in press, 2011.

Gupta, H. V., Beven, K., and Wagener, T.: Model calibration and uncertainty estimation, In: Anderson, M. G. (Ed.), Encyclopedia of Hydrological Sciences, John Wiley & Sons, Chichester, UK, 2005.

Hebeler, F. and Purves, R. S.: The impact of parametric uncertainty and topographic error in ice sheet modelling, J. Glaciol., 45, 899–919, 2008.

Helbig, N., Löwe, H., and Lehning, M.: Radiosity approach for the shortwave surface radiation balance in complex terrain, J. Atmos. Sci., 66, 2900–2912, 2009.

Idso, S. B. and Jackson, R. D.: Thermal radiation from the atmosphere, J. Geophys. Res., 74, 4167–4178, 1969.

Idso, S. B.: A set of equations for full spectrum and 8 to 14 µm and 10.5 to 12.5 µm thermal radiation from cloudless skies, Water Resour. Res., 17, 295–304, 1981.

Iqbal, M.: An Introduction to Solar Radiation, Academic Press, Toronto, Canada, 1983.

Iziomon, M. G., Mayer, H., and Matzarakis, A.: Downward atmospheric longwave irradiance under clear and cloudy skies: measurement and parameterization, J. Atmos. Solar-Terr. Phys., 65, 1107–1116, 2003.

JCGM: Evaluation of measurement data – Guide to the expression of uncertainty in measurement, Joint Committee for Guides in Metrology, Bureau International de Poids et Mesures, 2008.

Kasten, F.: A new table and approximate formular for relative optical air mass, Theor. Appl. Climatol., 14, 206–223, 1966.

Kavetski, D., Franks, S. W., and Kuczera, G.: Confronting input uncertainty in environmental modeling, Water Sci. Appl. Ser., 6, 49–68, 2003.

Klok, E. J. and Oerlemans, J.: A model study of the energy and mass balance of the Morteratschgletscher, Switzerland, J. Glaciol., 48, 505–518, 2002.

König-Langlo, G. and Augstein, E.: Parameterization of the downward long-wave radiation at the Earth's surface in polar regions, Meteorol. Z., 3, 343–347, 1994.

Konzelmann, T., van de Wal, R. S. W., Greuell, W., Bintanja, R., Henneken, E. A. C., and Abe-Ouchi, A.: Parameterization of global and longwave incoming radiation for the Greenland Ice Sheet, Global Planet. Change, 9, 143–164, 1994.

Leckner, B.: The spectral distribution of solar radiation at the Earth's surface–elements of a model, Solar Energy, 20, 143–150, 1978.

Lehning, L., Bartelt, P., Brown, B., and Fierz, C.: A physical SNOWPACK model for the Swiss avalanche warning Part III: meteorological forcing, thin layer formation and evaluation, Cold Reg. Sci. Technol., 35, 169–184, 2002.

Lhomme, J. P., Vacher, J. J., and Rocheteau, A.: Estimating downward long-wave radiation on the Andean Altiplano, Agric. Forest Meteorol., 145, 139–148, 2007.

Longman, R. J., Giambelluca, T. W., and Frazier, A. G.: Comparing the use of input parameters at different temporal resolutions, J. Geophys. Res., 117, D02201, doi:10.1029/2011JD016388, 2012.

Machguth, H., Purves, R. S., Oerlemans, J., Hoelzle, M., and Paul, F.: Exploring uncertainty in glacier mass balance modelling with Monte Carlo simulation, The Cryosphere, 2, 191–204, doi:10.5194/tc-2-191-2008, 2008.

Marshunova, M. S.: Principal characteristics of the radiation balance of the underlying surface, Soviet Data on the Arctic Heat Budget and its Climate Influence, Santa Monica, California, USA, 1966.

Marthews, T. R., Malhi, Y., and Iwata, H.: Calculating downward longwave radiation under clear and cloudy conditions over a tropical lowland forest site: an evaluation of model schemes for hourly data, Theor. Appl. Climatol., 107, 461–477, doi:10.1007/s00704-011-0486-9, 2012.

Marty, C. and Philipona, R.: The clear-sky index to separate clear-sky from cloudy-sky situations in climate research, Geophys. Res. Lett., 27, 2649–2652, 2000.

Maykut, G. A. and Church, P. E.: Radiation climate of Barrow, Alaska, 1962–1966, J. Appl. Meteorol., 12, 620–628, 1973.

Mittaz, C., Imhof, M., Hoelzle, M., and Haeberli, W.: Snowmelt evolution mapping using an energy balance approach over an Alpine terrain, Arctic, Antarctic, and Alpine Research, 34, 274–281, 2002.

Mulrooney, M. K. and Matney, M. J.: Derivation and application of a global albedo yielding an optical brightness to physical size transformation free of systematic errors, Advanced Maui Optical and Space Surveillance Technologies Conference, 12–15, 2007.

Nimielä, S., Räisänen, P., and Savijärvi, H.: Comparison of surface radiative flux parameterizations: Part I: Longwave radiation, Atmos. Res., 58, 1–18, 2001a.

Nimielä, S., Räisänen, P., and Savijärvi, H.: Comparison of surface radiative flux parameterizations: Part II: Shortwave radiation, Atmospheric Research, 58, 141–154, 2001b.

Okulov, O., Ohvril, H., and Kivi, R.: Atmospheric precipitable water in Estonia, 1990–2001, Boreal Environ. Res., 7, 291–200, 2002.

Oreopoulos, L. and Davies, R.: Plane parallel albedo biases from satellite observations. Part II: Parameterizations for bias removal, Am. Meteorol. Soc., 11, 933–944, 1998.

ORNL DAAC: Oak Ridge National Laboratory Distributed Active Archive Center, MODIS subsetted land products, Collection 5, ORNL DAAC, Oak Ridge, Tennessee, USA, 2010, available at: http://daac.ornl.gov/MODIS/modis.html, last access: March 2010.

Philipona, R., Fröhlich, C., and Betz, Ch.: Characterization of pyranometers and the accuracy of atmospheric longwave radiation measurements, Appl. Opt., 34, 1598–1605, 1995.

Philipona, R., Marty, C., Fröhlich, C., and Heimo, A.: Measurements of the longwave radiation budget in the Alps, in IRS 96: Current Problems in Atmospheric Radiation, edited by: Smith, W. L. and Stamnes K., A. Deepak Publishing, Hampton, Virginia, USA, 786–789, 1996.

Pirazzini, R., Nardino, M., Orsini, A., Calzolari, F., Georgiadis, T., and Levizzani, V.: Parameterization of the downward longwave radiation from clear and cloudy skies at Ny Alesund (Svalbard), in IRS 2000: Current Problems in Atmospheric Radiation, edited by: Smith, W. L. and Timofeyev, Y. A., A. Deepak Publishing, Hampton, Virginia, USA, 559–562, 2000.

Plüss, C. and Ohmura, A.: Longwave radiation on snow-covered mountainous surfaces, J. Appl. Meteorol., 36, 818–824, 1997.

Prata, A. J.: A new long-wave formula for estimating downward clearsky radiation at the surface, Q. J. Roy. Meteorol. Soc., 122, 1127–1151, 1996.

Reitan, C.: Surface dew point and water vapor aloft, J. Appl. Meteorol., 2, 776–779, 1963.

Robinson, G. D.: Notes on the measurement and estimation of atmospheric radiation, Q. J. Roy. Meteorol. Soc, 73,127–150, 1947.

Robinson, G. D.: Notes on the measurement and estimation of atmospheric radiation 2, Q. J. Roy. Meteorol. Soc, 76, 37–51, 1950.

Satterlund, D. R.: An improved equation for estimating longwave radiation from the atmosphere, Water Resour. Res., 15, 1649–1650, 1979.

Schillings, C.: Bestimmung langjähriger stündlicher Zeitreihen und räumlich hochaufgelöster Karten der Direkt-Normal-Strahlung auf der Basis von Meteosat-Daten und Atmosphärenparametern für die Nutzung in konzentrierenden Solarkraftwerken, Ph.D. thesis, Philipps-Universität Marburg, Marburg, Germany, 2004.

Sicart, J. E., Pomeroy, J. W., Essery, R. L. H., and Bewley, D.: Incoming longwave radiation to melting snow: observations, sensitivity and estimation in northern environments, Hydrol. Proc., 20, 3697–3708, 2006.

Spencer, J. W.: Fourier series representation of the position of the sun, Search, 2, 172 pp., 1971.

Staehelin, J., Renaud, A., Bader, J., McPeters, R., Viatte, P., Hoegger, B., Bugnion, V., Giroud, M., and Schill, H.: Total ozone series at Arosa (Switzerland): Homogenization and data comparison, J. Geophys. Res., 103, 5827–5841, 1998.

Swinbank, W. C.: Long-wave radiation from clear skies, Q. J. Roy. Meterol. Soc., 89, 330–348, 1963.

Wang, K. and Liang, S.: Estimation of daytime net radiation from shortwave radiation measurements and meteorological observations, Journal of Applied Meteorology and Climatology, 48, 634–643, 2008.

Wang, K. and Liang, S.: Global atmospheric downward longwave radiation over land surface under all-sky conditions from 1973 to 2008, J. Geophys. Res., 114, D19101, doi:10.1029/2009JD011800, 2009.

Yamamoto, G.: On nocturnal radiation, Sci. Rep. Tohoku Universitiy, 2, 27–43, 1950.

Zillman, J. and Commonwealth Bureau of Meteorology (Australia): A study of some aspects of the radiation and heat budgets of the Southern Hemisphere oceans, Meteorological Study, Canberra: Australian Government Publishing Service, 1972.